New Research in Ionizing Radiation and Nanoparticles: The ARGENT Project

Marta Bolsa Ferruz, Vladimir Ivošev, Kaspar Haume, Lilian Ellis-Gibbings, Ali Traore, Vivek Thakare, Soraia Rosa, Pablo de Vera, Vu-Long Tran, Arkadiusz Mika, Daria Boscolo, Sophie Grellet, Alexey Verkhovtsev, Bernd A. Huber, Karl T. Butterworth, Kevin M. Prise, Frederick J. Currell, Nigel J. Mason, Jon Golding, Emanuele Scifoni, Gustavo García, Frédéric Boschetti, F. Lux, O. Tillement, Cédric Louis, Kurt Stokbro, Andrey V. Solov'yov and Sandrine Lacombe

Abstract This chapter gives an overview of "ARGENT" ("Advanced Radiotherapy, Generated by Exploiting Nanoprocesses and Technologies"), an ongoing international Initial Training Network project, supported by the European Commission. The project, bringing together world-leading researchers in physics, medical physics, chemistry, and biology, aims to train 13 Early Stage Researchers (ESRs) whose research activities are linked to understanding and exploiting the nanoscale processes that drive physical, chemical, and biological effects induced by ionizing radiation in the presence of radiosensitizing nanoparticles. This research is at the forefront of current practices and involves many experts from the respective scientific disciplines. In this chapter, we overview research topics covered by ARGENT and briefly describe the research projects of each ESR.

S. Lacombe—On behalf of the ARGENT consortium, see http://www.itn-argent.eu.

M. Bolsa Ferruz (✉) · V. Ivošev · S. Lacombe
Institut des Sciences Moléculaires d'Orsay (ISMO), CNRS,
Univ. Paris-Sud, Université Paris-Saclay, 91405 Orsay Cedex, France
e-mail: marta.bolsa-ferruz@u-psud.fr

V. Ivošev
e-mail: vladimir.ivosev@u-psud.fr

S. Lacombe
e-mail: sandrine.lacombe@u-psud.fr

K. Haume · P. de Vera · N.J. Mason
Department of Physical Sciences, The Open University,
Milton Keynes MK7 6AA, UK
e-mail: Kaspar.Haume@open.ac.uk

P. de Vera
e-mail: p.devera@qub.ac.uk

N.J. Mason
e-mail: nigel.mason@open.ac.uk

K. Haume · P. de Vera · A. Verkhovtsev
MBN Research Center, 60438 Frankfurt am Main, Germany
e-mail: verkhovtsev@iff.csic.es

A.V. Solov'yov (ed.), *Nanoscale Insights into Ion-Beam Cancer Therapy*,
DOI 10.1007/978-3-319-43030-0_12

1 Introduction

Cancer remains a major health concern. Around 50 % of patients receive radiotherapy as part of their cancer treatment. The main limitation of this treatment is the lack of tumor selectivity, which causes severe side effects, and radioresistance. The most promising developments to improve the performances of radiation-based therapies are the use of fast ion-beam radiation (proton and carbon therapy) and nanoparticle-enhanced therapies.

The new FP7 European multi-ITN (Marie Curie Action Initial Training Network) project, named "Advanced Radiotherapy, Generated by Exploiting Nanoprocesses and Technologies" (ARGENT), has been in progress since March 2014. This project was built upon the strong foundations of the Nano-IBCT community and the "Nano-IBCT" COST Action [1]. The main objective of the intersectoral and multidisciplinary ARGENT ITN is to create a new generation of researchers and experts able to develop and propose to society new tools and concepts for the improvement of cancer therapy treatments.

ARGENT brings together world-leading researchers of different disciplines, namely, physicists and medical physicists, chemists, biologists, medical doctors, and small or medium-sized enterprises (SMEs), with the aim of understanding and exploiting the nanoscale processes induced by ionizing radiation. The consortium aims at training 13 Early Stage Researchers (ESRs) whose research activities are split into three work packages, entitled "Nanodosimetry", "Therapeutic Nanoagents", and

A.V. Solov'yov
MBN Research Center at Frankfurter Innovationszentrum Biotechnologie,
Altenhöferallee 3, 60438 Frankfurt am Main, Germany
e-mail: solovyov@mbnresearch.com

A.V. Solov'yov
A.F. Ioffe Physical-Technical Institute, Polytekhnicheskaya Ul. 26,
194021 Saint Petersburg, Russia

L. Ellis-Gibbings · A. Traore · A. Verkhovtsev · G. García
Instituto de Física Fundamental, Consejo Superior de Investigaciones Científicas,
Serrano 113-bis, 28006 Madrid, Spain
e-mail: l.ellisgibbings@csic.es

A. Traore
e-mail: traoredubuis@iff.csic.es

G. García
e-mail: g.garcia@iff.csic.es

V. Thakare · F. Boschetti
CheMatech, 9 Avenue Alain Savary, 21000 Dijon, France
e-mail: vivekthakare22@gmail.com

F. Boschetti
e-mail: fboschetti@chematech-mdt.com

V. Thakare
Institute of Molecular Chemistry, University of Bourgogne, Dijon, France

"Preclinical Evaluation". The ARGENT scientific objectives, which are the main concerns of these work packages, are the following:

- to advance understanding of the physicochemical processes initiated by the interaction of various forms of radiation with biological matter in the perspective to predict and control the effects of new treatments;
- to develop new nanodrugs able to direct and improve the application of these nanoscale phenomena for best patient benefit;
- to further the understanding of how the effects of these nanoscale phenomena can change clinical practice, and to evaluate the use of the new methods and tools developed in this project for better patient outcomes.

The "Nanodosimetry" unit combines experimental and computational techniques to answer the most fundamental questions regarding the mechanisms present in radiation-induced damage in cells. A group of ESRs study biomolecules, nanoagents and their mutual interaction when activated by slow and fast incident charged particles. This approach is crucial for the optimization of the interactions of potential nanodrugs with radiotherapy protocols.

The "Therapeutic Nanoagents" unit is composed of ESRs with a background in chemistry, pharmacy, biology and medical physics. This multi-disciplinary approach aims at synthesizing, characterizing and testing the properties and effects of potential new generation nanodrugs able to amplify radiation effects and to improve diagnostic performance. Cell uptake and localization of the nanoagents are also included to complete the investigation. The combination of nanoparticles with medical radiation

S. Rosa · K.T. Butterworth · K.M. Prise
Centre for Cancer Research and Cell Biology,
Queen's University Belfast, Belfast BT9 7AE, UK
e-mail: s.rosa@qub.ac.uk

K.T. Butterworth
e-mail: k.butterworth@qub.ac.uk

K.M. Prise
e-mail: k.prise@qub.ac.uk

P. de Vera · F.J. Currell
School of Mathematics and Physics, Queen's University Belfast, Belfast BT7 1NN, UK
e-mail: f.j.currell@qub.ac.uk

V.-L. Tran · F. Lux · O. Tillement
Team FENNEC, Institut Lumière Matière, UMR5306, Université Claude
Bernard Lyon1-CNRS, Université de Lyon, 69622 Villeurbanne Cedex, France
e-mail: vu-long.tran@univ-lyon1.fr

F. Lux
e-mail: francois.lux@univ-lyon1.fr

O. Tillement
e-mail: olivier.tillement@univ-lyon1.fr

V.-L. Tran · C. Louis
Nano-H S.A.S, 2 Place de l' Europe, 38070 Saint-Quentin-Fallavier, France
e-mail: c.louis@nano-h.com

(X-rays and fast ions used in radiation therapy) is studied from molecular to cellular scales, up to in vivo.

The "Preclinical Evaluation" unit combines their efforts to establish a link between nanoscale interactions and clinical effects, through investigating how nanoscale processes initiated by the interaction of radiation with living matter affect biological responses. Combining advanced experimental, theoretical and modeling tools, this team investigates nanoscale interactions for preclinical testing in cell-based models and explores their clinical applicability. The major goal of this team in ARGENT is to evaluate the use of the new methods and tools developed in the project for better patient outcomes.

This chapter provides an overview and background on activities that are being carried out within the ARGENT project. The chapter is organized as follows.

Sections 2–9 are devoted to experimental and theoretical studies of the properties of nanoparticles (NPs) proposed for radiation therapy applications and their interaction with cells. Section 2 introduces the idea of using NPs in radiation therapy and outlines different types of the systems used in ARGENT. Section 3 gives an overview of different techniques for the NP synthesis and characterization. Section 4 is devoted to functionalization of NPs by different ligands aimed for a better localization of NPs in tumors. Section 5 is devoted to the computational modeling of NPs and the investigation of their properties. Section 6 presents an overview of the NP toxicity studies. This problem is of crucial importance because the biological response induced by NPs is governed by physical and chemical properties that impact important cellular processes. Section 7 describes recent studies of the structure and stability of blood

A. Mika · B.A. Huber
Centre de Recherche sur les Ions, les Matériaux et la Photonique (CIMAP),
Unité Mixte CEA-CNRS-EnsiCaen-Université de Caen Basse-Normandie,
UMR 6252, 6 Boulevard Maréchal Juin, 14050 Caen, France
e-mail: mika@ganil.fr

B.A. Huber
e-mail: huber@ganil.fr

D. Boscolo · E. Scifoni
Biophysics Department, GSI Helmholtzzentrum für Schwerionenforschung GmbH,
Planckstraße 1, 64291 Darmstadt, Germany
e-mail: d.boscolo@gsi.de

E. Scifoni
e-mail: e.scifoni@gsi.de

S. Grellet · J. Golding
Department of Life, Health and Chemical Sciences,
The Open University, Milton Keynes MK7 6AA, UK
e-mail: sophie.grellet@open.ac.uk

J. Golding
e-mail: jon.golding@open.ac.uk

K. Stokbro
QuantumWise A/S, Fruebjergvej 3, 2100 Copenhagen, Denmark
e-mail: kurt.stokbro@quantumwise.com

proteins upon interaction with NPs. Section 8 provides a description of the cell lines which are used within ARGENT to perform experimental studies with different *in vitro* models. Section 9 describes the methods for measuring the NP uptake into different cells and makes an overview of preliminary results of the corresponding experiments.

The physical and chemical phenomena appearing due to interaction of biomolecular systems with ionizing radiation are the main topic of the research described in Sects. 10–13. Section 10 gives a background for particle track simulations along with a deeper discussion of the computer codes used in the project. Section 11 is devoted to the computational simulation of nanoscale shock waves induced by fast heavy ions traversing biological media. This mechanism of radiation damage may affect the distribution of free radicals and other reactive species formed after irradiation. The production of free radicals and the oxygen effect are described in Sect. 12. Section 13 describes experimental and theoretical methods for analyzing the effects of secondary species formed due to radiation on biomolecules and water.

Sections 14–16 are devoted to experimental and theoretical studies of the interaction of NPs with ionizing radiation and the impact of nanoscale phenomena on the resulting biological damage. Section 14 describes experimental studies of electron emission from ion-irradiated metallic NPs; the emission of low-energy secondary electrons induced by ionizing radiation is currently considered as one of the main mechanisms underlying the radiosensitizing properties of NPs. The impact of nanoscale processes on biodamage complexity is covered in Sect. 15. It describes some results obtained up to date towards the understanding of the physicochemical processes initiated by the interaction of various forms of ionizing radiation with biological matter. Section 16 describes the various modes of experimentation and pre-clinical trials to be undertaken by the ARGENT group—using both photon and ion radiation *in vitro* and in vivo. These studies should allow us to define optimal treatment protocols that are able to improve tumor treatment whilst decreasing the side effects on healthy tissue.

Finally, Sect. 17 briefly summarizes the different aspects covered in the chapter.

2 Exploration of Nanoparticles for Radiation Therapy Applications

Nanoparticles (NPs) represent the diverse set of colloidal structures that encompasses metals, inorganic materials (e.g., carbon or silica), peptides, proteins, bio- or synthetic polymers or hybrid compounds in conjugated or unconjugated forms. Although many different shapes have been reported, the spherical model has been widely studied and often discussed in this context with the expected size range of 10–100 nm. Nanoparticles having this size can be expected to be preferentially accumulated in the cancerous tissue owing to the widely cited phenomenon “Enhanced Permeation and Retention (EPR) Effect” [2].

Different aspects need to be taken into account when developing new NPs, such as the composition, size and shape, as well as surface coating and charge. These parameters can influence the uptake by cells, their biological response and interaction with radiation.

Metallic NPs composed of elements with high atomic number (high-Z elements) have been widely investigated because of strong electron emission after interaction with ionizing radiation, which is more pronounced as compared to small metal-containing molecular agents, good biocompability, an easy surface functionalization by attachment of ligands, and the possibility of synthesis in a wide range of sizes [3–9]. The use of NPs for radiosensitization was first demonstrated by Hainfeld et al. [10] using 1.9 nm gold nanoparticles (AuNPs) delivered systemically prior to irradiation in mice exhibiting mammary carcinomas. Other metal-based NPs made of platinum and silver have also been successfully used to radiosensitize cells although they are not as easily functionalized as gold, and silver has less biocompatibility and more toxicity [3, 6, 11–14]. Another choice is gadolinium which is used mainly for its contrast properties for magnetic resonance imaging (MRI). Gadolinium is toxic for cells and therefore must be chelated onto a core of another material such as polysiloxane or gold, thus reducing its cytotoxicity [15, 16] (see Sect. 3).

Some of the physical properties of NPs heavily influence their biological compatibility, effect and range. In this section, we detail some of the main properties that can be controlled in the synthesis process and the choice of NPs used within the ARGENT project.

2.1 Effects of Nanoparticle Size on the Uptake

The size of NPs used for radiosensitization not only affects how they interact with the biological system, but also how they interact with the radiation source. Moreover, biodistribution and the route of elimination from the body are also dependent on the NPs size.

Avoiding accumulation of NPs in non-targeted organs such as the heart and liver is a major concern as it may potentially cause long-term side effects; therefore, non-biodegradable NPs should be designed to be rapidly eliminated from the body. Elimination is mainly achieved through renal clearance, which has been demonstrated for NPs smaller than 6 nm [17–19].

Although experiments have a tendency to point to a maximum cell uptake of NPs between 20 and 60 nm [20–23], smaller NPs can accumulate in cancer tissues due to porous blood vessels near tumors [19]. Smaller NPs can diffuse further into tumor tissue and, therefore, present a more even distribution in larger tumors than larger NPs. This may counteract the fact that the actual cell uptake is less than that of larger NPs [20, 23]. Moreover, if the NPs are small enough, they can enter a cell directly by diffusion through the cell membrane [24].

In regards to the interaction between NPs and radiation, the latter interacts mostly with the interior of the NPs; therefore, if the NP size is increasing, the dose deposition of radiation in the medium from this interaction decreases [4]. Carter et al. [8] found that the production of low-energy electrons was larger for 3 nm NPs than for 6 nm NPs exposed to X-rays, and Lin et al. [25] found improved cell killing in their theoretical study of the X-ray and proton irradiation for 2 nm AuNPs compared to sizes up to 50 nm.

2.2 *Effects of Nanoparticle Charge on the Uptake*

The bi-lipid membrane of a cell is negatively charged, which has led to the suggestion that positively charged NPs might exhibit improved uptake due to electrostatic forces [20, 26–29]. However, the optimal charge on NPs for cell uptake is still unclear [26].

da Rocha et al. [30] simulated the uptake of differently charged NPs into cells and found that passive uptake (diffusion) was favored for neutral or slightly negatively charged NPs while for positively charged NPs endocytosis mediated uptake was dominant. Positively charged NPs have also been shown to interfere with certain cell functions, such as ion transport, and to perturb the membrane potential due to the stronger interaction between the positive NPs and the negative membrane [20, 26]. Furthermore, in vivo studies show that a positive charge of the NPs is associated with opsonization and therefore quicker elimination from the bloodstream [18]. However, this can be circumvented by properly coating the NP, as discussed below.

2.3 *Active and Passive Targeting*

To specifically target tumor tissue, the coating of NPs is an indispensable tool and can be used in mainly two ways: passive targeting and active targeting [31], which are discussed below.

Passive targeting relies on EPR and the fact that tumor tissue tends to see higher uptake of macromolecules (e.g., NPs) from the bloodstream due to the presence of leaky vasculature and reduced lymphatic clearance from the tumors compared to healthy tissue [17]. The abnormal blood vessel growth near tumors, induced by these cells' growth mechanisms, create pores in nearby healthy blood vessels [32]. The size of the pores can be as large as 200–1000 nm which allows NPs to extravasate the blood vessels and accumulate in the tumor. In addition, tumor tissue has subnormal lymphatic clearance, which means that anything that is absorbed tends to be retained for longer [32].

In the body, specialized opsonin proteins found in blood serum tend to adsorb onto the surface of any foreign substance, labeling it for clearance from the body [7]. To take advantage of the random uptake during passive targeting, a protracted bloodstream circulation time is required. It has been shown that NPs coated with the

molecule poly(ethylene glycol) (PEG) reduces opsonization, thereby increasing the NP circulation time by effectively giving it a "stealthy" nature [17, 33]. The mechanism for the reduced opsonization has been linked to a repelling force from the PEG molecules when opsonins attempt to adsorb and cover the NP [34, 35]. The uptake dynamics of NPs changes when they become covered by opsonins [36]. The reduced interaction granted by a PEG coating thus ensures that uptake properties are more controllable [34, 37].

Active targeting involves the attachment of molecules on the NPs for which suitable receptors exist on the surface of cancer cells. One example is the growth factor Her2, which is overexpressed in a large portion of human breast cancers. By attaching the antibody anti-Her2, NPs can be specifically targeted towards these cells [38].

Another, more general, kind of targeting exploits the higher and faster proliferation of cancer cells compared to healthy cells. The increased growth of cancer cells requires more glucose for their metabolism, therefore glucose-coated NPs tend to have a higher interaction with cancer cells [39–41].

It is also possible to combine passive and active targeting by coating NPs with a combination of PEG and a targeting molecule. However, this requires carefully balancing the two coating molecules: too much PEG will reduce the effect of the targeting molecule, whereas too much targeting molecule will reduce the circulation time [38]. Furthermore it has been shown that the length of the PEG molecules should not exceed the length of the targeting molecules to avoid hindering their interaction with their targeted receptors [42].

2.4 Nanoparticles Used in ARGENT

ARGENT industrial partners, Nano-H and Chematech, have developed 3 different NPs, named Au@DTDTPA, Au@DTDTPA-Gd and AGuIX (see Fig. 1). Au@DTDTPA are gold-based NPs with a ∼2.4 nm core coated by dithiolated diethylenetriamine pentaacetic acid (DTDTPA), presenting ∼6.6 nm of total diameter (Fig. 1a). These NPs have shown encouraging experimental results in combination with ionizing radiation (see Sect. 16). To improve the imaging and possibly the radiosensitizing potential, the Au@DTDTPA NPs were chelated with gadolinium ions (Fig. 1b). The Au@DTDTPA-Gd50 NPs (50 ions of gadolinium per NP) promote a contrast enhancement in MRI and the gadolinium ions do not change the size of the particles since there is no change in the spectrum of the gold NPs colloid [18]. These NPs have shown promising results with low toxicity, theranostic (therapeutic + diagnostic) properties, and easy excretion from the body [18, 43].

AGuIX (Activation and Guidance for X-ray Irradiation) are ultrasmall (under 5 nm) NPs that are made up of a polysiloxane core grafted with Gd^{3+} DOTA (1, 4, 7, 10-tetra-azacyclododecane-1-glutaric anhydride-4, 7, 10-triacetic acid) chelates and primary amines (Fig. 1c). The AGuIX NPs can also be used for theranostics as they can be imaged by both MRI and CT scan [19]. Experimental studies performed by

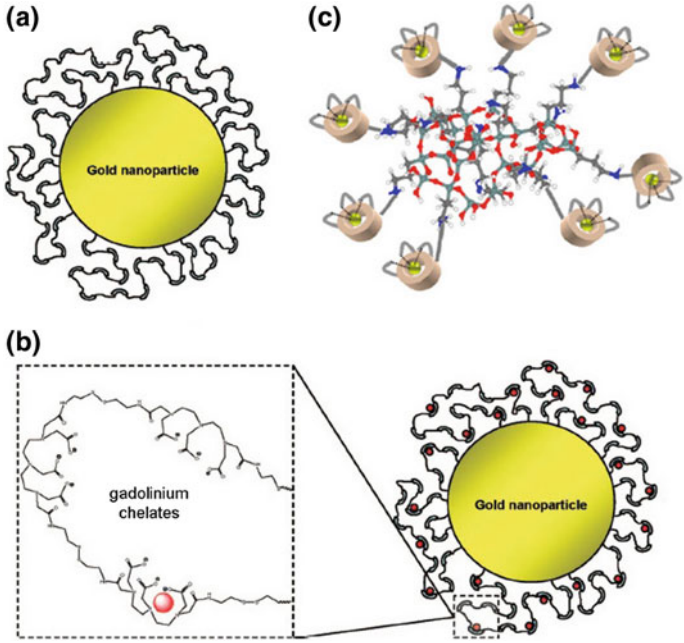

Fig. 1 Au@DTDTPA (**a**), Au@DTDTPA-Gd (**b**) and AGuIX (**c**) nanoparticles which are studied experimentally within the ARGENT project. Figures are adapted from Refs. [16, 19]

ESRs within the ARGENT project are mostly carried out with these three types of NPs. Small platinum NPs with the size of less than 5 nm are also tested; a radioenhancement effect produced by these NPs was demonstrated earlier [3].

3 Synthesis and Characterization of Nanoparticles for Cancer Treatments

3.1 Synthesis Methods

"Metal based nanoparticles for biomedical applications" is a very wide field of research including many different structures published in literature. Therefore, a very wide range of synthesis methods have been introduced to date, as summarized in Fig. 2. Generally, the first step is the synthesis of a metal or a metal oxide core. The second step is usually the formation of a coating around the core for biocompatibility.

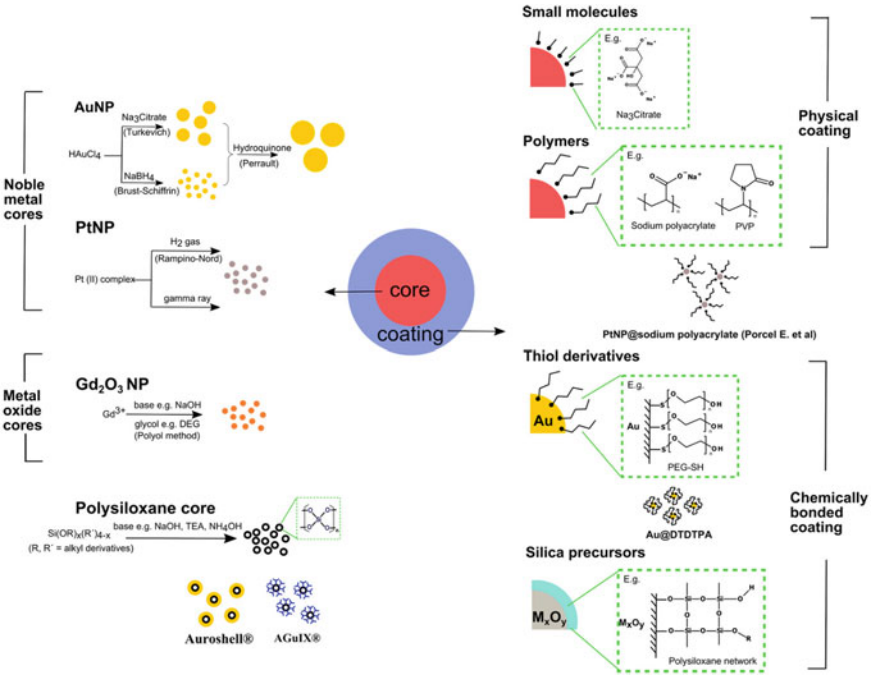

Fig. 2 Illustration of various methods for synthesizing and coating some inorganic nanoparticles used for radiosensitization in cancer therapy

3.1.1 Methods for Synthesizing Metal Cores

For noble metals, such as gold (Au) or platinum (Pt), the most common methods are the reduction of respective salts by different reductants to create metal particles [3, 44]. Gold nanoparticles (AuNPs) can be synthesized from $HAuCl_4$ mainly by three methods depending on the targeted size [44]. The first method to produce AuNPs was proposed by Turkevich et al. [45, 46]; this produces NPs in the range from 15 to 150 nm using citrate as a reducing agent. Ultrasmall AuNPs of less than 10 nm can be achieved from the method described by Brust-Schiffrin [47] with $NaBH_4$ as reductant and alkylthiols as stabilizers. The AuNP coated by DTDTPA, one of the nanoparticles commonly used in the ARGENT project (see Fig. 1a), is an example of this method [48]. Bigger NPs might be achieved with the Perrault method which utilizes hydroquinone to slowly reduce Au(III) onto small AuNP seeds [49]. Pt nanoparticles (PtNPs) are classically synthesized from K_2PtCl_4 using hydrogen gas as the reducing agent [50]. Different kinds of polymers such as sodium polyacrylate, polyvinylpyrrolidone (PVP) or ethylene glycol are used to stabilize the solution [51]. Porcel et al. [3] have applied a radiolytic reduction method using γ-rays to synthesize ultrasmall PtNPs of ca. 3 nm; these NPs are studied in ARGENT

as radiosensitizers. In the cited work, radiolytic reduction of platinum complexes was performed in an aqueous solution, containing or not different polymers used as a coating [3].

3.1.2 Methods for Synthesizing Metal Oxide Cores

For other heavy metals, e.g., for gadolinium (Gd), oxide cores are mostly created from their salts [52]. Gd_2O_3 particles are usually produced by reacting $GdCl_3$ or $Gd(NO_3)_3$ with sodium hydroxide in polyethylene glycol (PEG) or diethylene glycol (DEG). This method called "polyol approach" takes advantage of the high viscosity and high boiling temperature of polyols to prevent the aggregation of particles and induce thermolysis of hydroxide into oxide [53, 54].

3.1.3 Methods for Coating Metal Based Nanoparticles

It is almost impossible to use metal NPs in biological medium without a biocompatible coating, due to the fact that metal oxides like Gd_2O_3 can be easily dissolved in water to produce toxic Gd^{3+} ions. Even with inert and biocompatible materials such as Au or Pt, a coating layer might offer higher colloidal stability which leads to longer shelf life and stealth effect which prevents protein adsorption, macrophage clearance and finally liver accumulation [55]. Normally, AuNPs are naturally coated with a layer of citrate or alkylthiols after the synthesis based on the Turkevich or Brust method, respectively. However, these layers are either quite weakly bonded (citrate) or hydrophobic (alkylthiols) and therefore not biocompatible. The most commonly used material for coating is PEG [56]. On AuNP, mercaptopolyethyleneglycol (PEG-SH) can be readily used [57]. A wide range of macromolecules, i.e., natural and synthetic polymers or dendrimers, have also been used as thiol derivatives to coat AuNP [56]. In the case of metal oxides, silane precursors can be used to form stable chemically bonded silica coating layers on their surfaces [54, 58]. Other polymers, e.g., oleic acid or PVP have also been reported to form stable coatings on Gd_2O_3 surface [59].

In some studies, the coating layer may provide other functionalities. For example, in Au@DTDTPA NPs, the gold core is coated by a layer of dithiol DTPA, a strong chelator which can be used later to incorporate Gd^{3+} or radioisotopes such as ^{111}In or ^{99}Tc in order to turn the particle into an efficient MRI contrast agent and gamma emitters for scintigraphy [18].

3.1.4 Methods for Synthesizing Silica Cores

Instead of metal and metal oxide cores, other authors have created silica nanoparticles (SNPs) and coated them with metals, for example gold as in Auroshell® [60], or functionalized them with different chelators which strongly coordinate metals [61].

There are two main methods used to synthesize SNPs, namely the Stober method and water-in-oil microemulsion [62]. The former is based on the hydrolysis-condensation reaction of a silane precursor catalysed by bases, e.g., ammonia in mixtures of water and alcohol to form polysiloxane 3D networks [63]. This technique is simple and easy to scale up but unable to create homogeneous SNPs under 10 nm. However, recently, different terminating approaches have been introduced to achieve ultrasmall SNPs [64, 65]. The microemulsion approach is basically the Stober process carried out in tiny water droplets separated by oil and surfactants. Although this method is believed to be able to produce homogeneous small SNPs, it suffers from a complicated and time-consuming purification procedure to get rid of the oil and surfactants [66].

Gadolinium-based AGuIX NPs (Fig. 1c) are produced from an original top-down approach starting from a conventional Gd_2O_3 NP coated with a silica layer functionalized by DOTA, a macrocycle chelator which is very stable and commonly used for Gd^{3+}. The presence of DOTA, a thin silica coating layer and an acidic synthesis solution accelerate the dissolution of Gd_2O_3 core, break down the silica coating layer into pieces and allow Gd^{3+} ions to be chelated by DOTA finally leading to the stable AGuIX NP [61]. A description of the AGuIX structure and properties by different analytical tools as well as an exploration of the synthesis and functionalization of these NPs are the main topics of the ESR research project "Development of lanthanides based nanosensitizers for theranostics", carried out by Vu-Long Tran in Lyon, France. His project is supervised by François Lux and Olivier Tillement (University Lyon I) and Cédric Louis (Nano-H).

3.2 Characterization Techniques

As with synthesis methods, a very wide range of characterization techniques have also been developed and adapted in order to control the quality of the NPs. Some of these techniques are classified and briefly described below according to the characteristics of the particles they are able to characterize.

3.2.1 Determination of Particle Size and Shape

The size of NPs can be determined by several techniques. The most straightforward method is scanning/transmission electron microscopy (SEM/TEM) which offers direct observation of the size of particles. However, this technique requires complicated equipment and sample preparation [67]. Meanwhile, the most commonly used method is dynamic light scattering (DLS) which deduces the diffusion coefficient of the particles in the solution from the correlation function of scattering light intensity over time. Then, the hydrodynamic radius of the particle, which is the radius of a hypothetical hard sphere that has the same diffusion coefficient as the particle, can be calculated from the Stokes-Einstein equation [68]. Another optical spectroscopy technique that is used to measure particle size is small angle X-ray scattering (SAXS).

This method allows determination of the radius of gyration which is defined as the root-mean-square distance of all elemental scattering volumes from their center of mass weighted by their scattering densities [67]. Diffusion ordered nuclear magnetic resonance spectroscopy (NMR DOSY) can also be described as a method for size determination. This technique utilizes an encoding/decoding process of the nuclear magnetization by spin-echo pulses to probe translational diffusion so that the result will be a 2D plot of diffusion coefficients and chemical shifts of studied nuclei e.g. ^{1}H, ^{13}C or ^{29}S [69, 70]. Through diffusion coefficients, hydrodynamic diameter can be inferred again from the Stokes-Einstein equation. However, this method cannot be used to study paramagnetic materials such as Gd because they can dramatically shorten the relaxation time and broaden the width of chemical shift peaks so that it makes the encoding process impossible to achieve. In reality, several methods need to be exploited in order to have a precise idea about the size of particles [71]. Some of the above techniques might be used also to determine their shape. SEM/TEM can undoubtedly reveal the morphology of particles. Also, the ratio between radius of gyration and hydrodynamic radius can give an idea of the particle morphology [67].

3.2.2 Determination of Overall Elemental Composition, Mass and Morphology

Another level of control highly demanded in the case of NPs is the knowledge of elemental composition and crystallinity. The former can be investigated with standard methods such as inductively coupled plasma mass spectrometry (ICP-MS), inductively coupled plasma optical emission spectroscopy (ICP-OES) or X-ray photoelectron spectroscopy (XPS). Meanwhile, the average mass of NPs can be determined by electrospray ionization (ESI) or matrix assisted laser desorption ionization (MALDI) mass spectrometry. These data may help to establish the average molecular formula of the particles. Interestingly, in the case of AGuIX, STEM was used with high-angle annular dark-field imaging (HAADF) and electron energy loss spectroscopy (EELS) imaging approaches to visualize different elements within individual particles [61]. The crystallinity of the particles, especially their core in core-shell structures, might be answered by high resolution transmission electron microscopy (HRTEM) or X-ray diffraction [72].

3.2.3 Determination of Surface Charge

Surface charge of nanoparticles can be determined by measuring the zeta potential existing between the first ion layer surrounding a particle and the ions in solution [68].

3.2.4 Detection and Quantification of Functionalized Ligands

Existing NPs in the literature are highly varied in terms of functionalized ligands. Hence, numerous techniques have been utilized to quantify the ligands of interest including thermogravimetric analysis (TGA), chemical assays, infra-red spectroscopy (IR), NMR and MS. In functionalized inorganic NPs, TGA can be used to determine the presence and quantity of organic content by weight loss as a function of increasing temperature. This method has been applied for Au@DTDTPA [48]. However, this technique cannot give precise structural information about the grafted functions. Chemical assays such as the quantification of free DOTA by Eu^{3+} used in AGuIX development can be a very useful approach [61]. Nevertheless, this technique requires handling many samples. Therefore, it might be time and material consuming. IR is a handy and well developed technique that allows detection of chemical changes by the shift of the infrared absorption band of material. This approach is very frequently used in literature for detecting functionalized ligands and has also been used for AGuIX and Au@DTDTPA but is hardly quantitative [48, 73, 74]. Similarly, MS can hardly be used as a quantitative method due to its complicated procedure of nebulization, ionization, ion selection and detection although it is a powerful qualitative technique for determining the grafting of ligands [73, 74]. Finally, NMR is a technique with great potential for both detecting and quantifying the grafted organic functions on particles as long as the spectra are not too complicated to have good peak resolution. Interestingly, with the NMR-DOSY technique, the presence of organic ligands can be directly correlated to the integrity and the size of the particle. This allows a straightforward approach for evaluating the stability of degradable NPs [61]. However, as previously mentioned, it is limited to non-magnetic materials.

3.2.5 Evaluation of Stability, Purity and Degradation

Since NPs applied in the biomedical field are strictly regulated, their stability, purity and degradation are of great importance and can be evaluated by high performance liquid chromatography (HPLC) in combination with optical detectors (UV-Vis, Fluorescence) or MS, as shown in the work of Truillet et al. [75].

3.2.6 Characterization of AGuIX and Au@DTDTPA Nanoparticles

Specific NPs might be evaluated very differently in terms of efficacy depending on their applications. In the case of radiosensitizers, no ready method has been developed to test the radiosensitization effect before in vitro and in vivo studies. However, with theranostic NPs such as AGuIX and Au@DTDTPA, their efficiency as contrast agents might be rapidly tested with relaxometry. This gives the value of longitudinal relaxivity, r_1, and transverse relaxivity, r_2. Higher r_1 indicates better efficacy as positive contrast agents [77].

Table 1 Summary of AGuIX and Au@DTDTPA characterization

No.	Characteristics	Nanoparticle			
		AGuIX	References	Au@DTDTPA	References
1	Hydrodynamic radius (R_h) by DLS	1.4 ± 0.3 nm	Unpubl.	Core: 1.2 ± 0.3 nm whole: 3.3 ± 0.9 nm	Alric C et al. [18]
2	Diameter of gyration (R_g) by SAXS	1.4 ± 0.1 nm	Unpubl.	N/a	
3	Ratio R_g/R_h	1		N/a	
4	Hydrodynamic radius (R_h) of Y^{3+} alternative by DOSY	~2.3 nm	Unpubl.	N/a	
5	SEM/TEM image	Yes	Mignot et al. [61]	Yes	Alric et al. [18], Debouttiere et al. [48]
6	X-ray Diffraction	N/a		Yes	Debouttiere et al. [48]
7	Elemental analysis by ICP-MS	%Gd: 14.0; %Si:11.5; %C: 29.0; %N: 8.1	Unpubl.		
8	Elemental analysis by XPS	N/a		Ratio of elements	Debouttiere et al. [48]
9	Zeta potential at pH 7.4	9.03 ± 5.5 mV	Kotb et al. [76]	−30 mV	Debouttiere et al. [48]
10	Mass	~8.5 ±1 kDa	Kotb et al. [76]	N/a	
11	Chemical composition	$Gd_{10}Si_{40}C_{200}$ $N_{50}O_{150}Hx$	Kotb et al. [76]	N/a	
12	Thermogravimetric analysis	N/a		150 DTDTPA ligands per particle	Debouttiere et al. [48]
13	Purity by HPLC UV detector	>95 %	Unpubl.	N/a	
14	Lifetime at pH 7.4 by HPLC-MS	3 h	Truillet et al. [75]	N/a	
15	Longitudial relaxivity r_1	9.4 $s^{-1}mM^{-1}$ at 60 MHz	Sancey et al. [19]	9.4 $s^{-1}mM^{-1}$ at 60 MHz	Miladi et al. [52]
16	Ratio r_2/r_1	1.14 at 60 MHz	Sancey et al. [19]	1.3 at 60 MHz	Miladi et al. [52]

Many of the techniques described above have been applied to AGuIX and Au@DTDTPA NPs that are used in the ARGENT project. The results of characterization of these NPs are summarized in Table 1.

4 Functionalization of Nanoparticles for Tumor Targeting and Biocompatibility

Active targeting of nanosized structures is an exciting avenue in terms of adding the exceptional ability of localization into tumor tissue. Active targeting harnesses the capability of affinity ligands to selectively bind to the receptors predominantly overexpressed on the cancer cells. The approach based on the premise of the "Magic Bullet" is aimed towards maximizing the interactions between NPs and cells, thus augmenting the internalization of NPs containing drugs without altering its overall biodistribution [78]. This section details the importance and options for targeted ligand attachment, the various methods for conjugation of ligands, and the status and future outcomes of using nanomedicines for targeted therapeutic treatments.

At present, active targeting has been a widely pursued strategy to complement the enhanced permeation and retention (EPR) effect and further enhance the efficacy of nanomedicine. The current research in the context of nanomedicine is mainly dedicated towards the delivery of chemotherapeutic drugs in the oncology space. The ARGENT program aims to widen the scope of nanomedicine through the development of nanotechnological tools to improve the outcome of the radiotherapy, which so far has not been rigorously investigated. The ESR research project "Nanoagent functionalization aiming at tumor targeting and biocompatibility" is carried out by Vivek Thakare at Chematech and University of Bourgogne (Dijon, France) under the supervision of Frederic Boschetti (Chematech) and Franck Denat (University of Bourgogne). The project is focused on the development of novel strategies to synthesize NPs for the imaging and therapy of cancer. The project also aims to conjugate these NPs with suitable bio recognized ligands so as to selectively dart the cancerous tissue. Such an approach demands substantial manipulation and investigations at the chemical/biophysical level.

4.1 Targeting Ligands

Active targeting encompasses anchoring the affinity ligands onto the surface of the NPs. These ligands could be small molecules such as sugars, lipids, peptides, proteins, antibodies or antibody fragments. The design of actively-targeted NP drug carriers is an intricate affair owing to the NP's supramolecular architecture, the ligand conjugation chemistry and the several types of ligands at scientists' disposal. The key determinants for the development of ligand based nanotherapeutics include: the

target/receptor on the cancer cells of interest, surface chemistry of the nanoparticles, ligand structure and the associated linker chemistry [79].

Several factors determine the success of active targeting, however the basic premise is that the NP needs to reach sufficient concentration at the cancerous site so as to affect the advantage of ligand conjugation. In most of the instances, particularly with smaller ligands, the pharmacokinetics and biodistribution of the NPs may not be affected and hence they form the best choice. However, off target accumulation of the targeted NPs may occur in cases where the receptors for the ligands are also expressed in the healthy tissue (e.g., folic acid). To some extent this can be resolved through the use of highly specific ligands like monoclonal antibodies.

From the viewpoint of ARGENT, it is interesting to integrate different modalities to sensitize cancer cells to the ionizing radiation. For instance, chemotherapeutic platinum based drugs like cisplatin have been shown to improve radiotherapy through their synergistic effects on the DNA damage [80]. Monoclonal antibodies also exhibit their ability to sensitize cells to ionizing radiation through their effects on the subcellular machinery [81]. The project delves to integrate the above modalities into nanoparticulate platform so as to harness and maximize their synergy.

4.2 Conjugation Strategies

Bioconjugate chemistry used for the grafting of ligands on the NP surface is typically based on aqueous reactions owing to instability of the NPs/ligands in organic solvents. One widely explored strategy is the so-called "EDC-NHS" chemistry, which involves activation of the carboxylate groups on the NP surface with a zero length linker 1-Ethyl-3-(3-dimethylaminopropyl) carbodiimide hydrochloride (EDC) and ester/intermediate stabilizer N-Hydroxy Succinimide (NHS) followed by reacting it with the amine group present on the ligand (Fig. 3a). The reaction can be performed vice-versa depending on the functional groups present on the NP or ligands. The efficiency of the reaction depends on the pH of activation and coupling, ratio of NP/ligand concentration and concentration of activating agents [82].

Another strategy that has found widespread mention is the maleimide chemistry (Fig. 3b). The focus on this chemistry has gained relevance owing to the increased number of approved biologics/protein based drugs which could also be used as ligands (e.g., monoclonal antibodies). The reaction involves the maleimide group (typically present on NPs) and the thiol group (typically present on protein/peptide ligands) resulting in the formation of the 3-thiosuccinimidyl ether bond. If free thiol groups are not present on the proteins they could be generated through partial reduction of proteins or through thiolation using Traut's reagent or other thiolation strategies [84].

"Click chemistry" (Fig. 3c) also deserves a mention here, although it is not as popular as the above two methods owing to the synthetic modifications required for both the ligands and the NP. The copper(I)-catalyzed azide-alkyne cycloaddition (CuAAC) occurs in the presence of copper(II) (e.g., copper(II)sulfate) and a

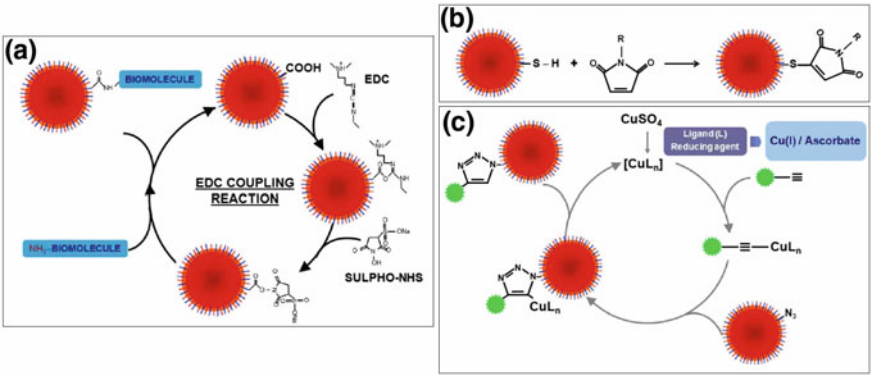

Fig. 3 Conjugation strategies: EDC-NHS coupling chemistry (**a**), maleimide-thiol chemistry (**b**), and click chemistry (**c**). The figure is adapted from Ref. [83]

reducing agent (e.g., sodiumascorbate) to produce Cu(I) in situ and is regarded as a bioorthogonal chemistry for site specific bioconjugation. Azides and alkynes are highly energetic functional groups with selective reactivity resulting in the formation of triazole providing good yields hence referred to as "click chemistry". The reaction occurs at room temperature, showing a high degree of solvent and pH insensitivity and high chemoselectivity [85].

4.3 Future Challenges in Nanomedicine Development

Nanomedicine is a burgeoning field with a diverse set of applications across several disease areas, but so far the progress witnessed in the oncology space has been overwhelming. More than half a dozen products are already approved while many more are undergoing clinical trials. These products mainly address the drug delivery issues with the chemotherapeutic drugs, however it should not be surprising to see the applications in imaging or theranosis making their headway. With the advances in the immunological tools for cancer therapy, the biologics/protein based drugs have assumed a prominent role in adding value to nanomedicine and represent an integrated approach towards developing targeted therapeutics. In the future, nanomedicine has the potential to improve the outcome of radiotherapy through its complex interactions with biological systems, which remain to be fully elucidated and explored. The objective of ARGENT is to steer in this direction, so as to contribute to maximizing the outcome of radiotherapeutic strategies. However, development of nanomedicines is bridled with several challenges in terms of the manufacturing, the biological efficacy and the lack of an established approval pathway unlike other conventional drugs. At the chemistry, manufacturing and control (CMC) level, the challenge is to produce nanomaterials that are rigorously characterized and repro-

ducible across all scales. Moreover, this needs to be strongly justified through the stringent safety and efficacy data from clinical trials that validate the potential of such nanometric tools over the existing standard therapeutics. Nonetheless, the pace at which the advances in this field have been made certainly forecast nanomedicine to be a bright spot in the future of cancer therapy and diagnosis.

5 Computational Modeling of Nanoparticle Coatings and Shapes

The coating and the shape of nanoparticles (NPs) is a crucial tool in manipulating their properties and behavior [6]. Due to the vast number of parameters involved in optimizing the shape and the composition of NPs (e.g., which coating molecules to use, how many, should they have a specific charge), it is a daunting task to systematically go through each of them experimentally. Modeling the different parameters with computer simulations can provide a significant speedup in this process.

5.1 Modeling of Coatings

The ESR project "Development of new modules for ATK code for modeling radiosensitizing nanoagents" is carried out by Kaspar Haume at the Open University (Milton Keynes, UK) in close collaboration with MBN Research Center (Frankfurt am Main, Germany) and QuantumWise (Copenhagen, Denmark). This work is coordinated by Nigel Mason (The Open University), Andrey Solov'yov (MBN Research Center) and Kurt Stokbro (QuantumWise). The research project aims to study the structure and behavior of the coating on NPs intended for use in cancer treatment. One of the tasks is to determine the optimal number of coating molecules to obtain a realistic system, one suitable for further simulations regarding the interaction of these NPs with radiation and the intracellular environment. Currently, the focus is on 1.5 nm gold nanoparticles (AuNPs) coated with polyethylene glycol (PEG).

In the simulations, between 32 and 60 PEG molecules are attached to the AuNP, and the system is then annealed from 1000 K down to 0 K. In this way, we can make sure that the coating molecules have had enough energy to overcome local barriers, and have been free to attain their optimal structure. Additionally, by doing this, we can extract information about the behavior of the coating at intermediate temperatures not just related to body temperature (310 K).

In this project, classical molecular dynamics (MD) simulations are employed to model the structure and behavior of the coating of NPs for different combinations of NP material, shape and size, and coating molecules [86].

Classical MD is basically the solution of Newton's equations of motion for a set of atoms. From an initial starting point, forces are calculated on all atoms, which leads to

an acceleration on all atoms as given by Newton's law, $\mathbf{F} = m\mathbf{a}$. By integration of the acceleration with respect to time (for given infinitesimal time steps $\mathrm{d}t$), new positions are given to all atoms and the process starts again. Temperature effects are included by perturbing the equations in a suitable way, given by the used thermostat. More specifically, the positions of atoms are updated by solving the following equation, known as the Langevin equation [87]:

$$m_i \frac{\mathrm{d}^2\mathbf{r}_i}{\mathrm{d}t^2} = \sum_{j \neq i} \mathbf{F}_{ij} - \frac{1}{\tau_\mathrm{d}} m_i \mathbf{v}_i + \mathbf{f}_i, \tag{1}$$

where $\sum_{j \neq i} \mathbf{F}_{ij}$ is the total force acting on atom i as a consequence of its interaction with all the rest of atoms j (i.e., second Newton's law). The second and third terms in the right-hand side of Eq. (1) correspond to the thermostat, used to keep the temperature of the system nearly constant to T, when coupled to a thermal bath. In the simulations performed within the project of Kaspar Haume, the Langevin thermostat is used, which acts as a viscous force on each particle of velocity v_i. τ_d is the damping time of the thermostat, while f_i is a random force with zero mean and dispersion $\sigma_i^2 = 2m_i k_\mathrm{B} T/\tau_\mathrm{d}$, with k_B being the Boltzmann's constant.

The force in Eq. (1) is given by the applied force field, which takes into account various parameters, such as bond distance, bond angle, and others. Utilizing a suitable force field for the given task is a crucial part of doing good MD simulations.

For biomolecular systems, which are the topics of interest in ARGENT, the structure of the molecules is not only dominated by interatomic distances, but also by the geometric configuration of groups of atoms, due to the molecular orbital hybridization. In this case, it is common to use specialized force fields describing such interactions, such as the CHARMM force field [88], which is one of the most commonly used force fields for describing the interactions of biomolecules. The force acting on the atom i is obtained from the potential energy $U(\mathbf{R})$ as $\sum_{j \neq i} \mathbf{F}_{ij} = \mathrm{d}U(\mathbf{R})/\mathrm{d}\mathbf{r}_i$, which corresponds to a given set of atomic coordinates R, and is expressed as a combination of energies arising from the distances of bonds between pairs of atoms, the angles formed between groups of three sequentially bonded atoms, the dihedral and improper angles formed by groups of four bonded atoms, and the non-bonded interactions, represented by the pure Coulomb force and the van der Waals interaction between pairs of atoms.

One of the parameters we monitor is the radius of the system versus the number of coating molecules, see Fig. 4. It is clear from the figure that the radius of the coated NP increases with increasing number of coating molecules and for increasing temperature of the system. The increase with number of coating molecules is related to the mutual repulsion of the molecules. The PEG molecule is composed of a C–C–O backbone which makes it almost linear in its native state. By increasing the coating concentration, the PEG molecules will repel each other and enter an increasingly linear structure, to increase their mutual distance, which leads to a larger radius of the system.

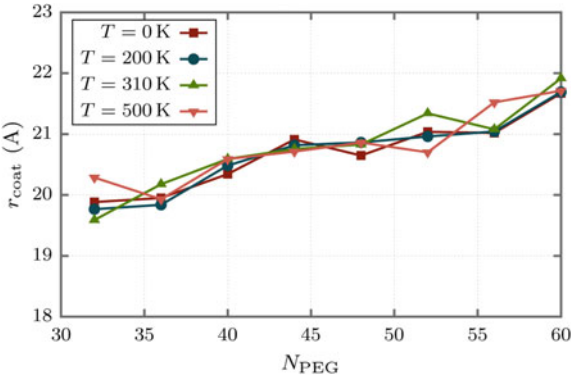

Fig. 4 The radius of the system as a function of the number of coating PEG molecules

The increase in radius for increasing temperature is likely related to the mutual interactions as well. Increasing the kinetic energy of the PEG molecules will increase the interaction between them, and this is again reduced by attaining a more linear structure.

Other results from simulations include the density distribution of the coating, the penetration of water molecules into the coating, the energetic stability of the coating, and more. All of this will aid in enabling future calculations of electron production under irradiation, propagation of electrons through the coating, and interaction with biological compounds of the cell such as proteins and DNA.

5.2 Impact of the Nanoparticle Shape on Its Electronic Properties

Within ARGENT, one of the goals is to investigate how shape and size influence the yield of electrons emitted from radiosensitizing NPs. In the ESR project "Validation of low energy scattering model in medical radiation planning", carried out by Ali Traore at CSIC (Madrid, Spain) under the supervision of Gustavo Garcia, this problem is partially covered by performing the simulations of the electromagnetic properties of irradiated AuNPs. Using the Metallic Nanoparticle Boundary Element Method (MNPBEM) toolbox of Matlab, it is possible to calculate the electron energy loss spectra (EELS) which give information about the electron yield; the latter is related to the radiosensitization efficiency of NPs [89, 90]. The goal of this work is to determine the size and the shape which provides the highest efficiency in terms of electron yield.

Up to date, this study has considered a 60 keV electron beam, primarily for validation with existing experimental data available at that energy [89]. The study of electromagnetic properties is performed by solving the classical Maxwell equations around the NPs. EELS of AuNPs were computed from the surface charges and cur-

rent distribution calculated with the BEM approach at the NP boundaries embedded in a water dielectric environment [91]. The BEM method is based upon a rigorous numerical solution of Maxwell's equations in the Fourier domain, assuming that the materials involved in the structure are described in terms of frequency-dependent dielectric functions. The dielectric functions of gold were extracted from the handbook of optical data and the Drude-Lorentz formula [92] and the impact parameter was taken equal to 5 nm.

For several sizes of gold NPs three distinct geometries have been investigated, namely a sphere, a rod, and a torus with equivalent volumes determined by the nanosphere radius (Fig. 5). These various structural shapes should give insights into other types of geometry. Preliminary results demonstrate that the NP's geometry affects the EELS of AuNPs. Among the shapes investigated, the metallic structure in the form of a rod yields the highest EEL spectrum. Future work will be devoted to the analysis of the coating effects on electron production following the methodology schematically illustrated in Fig. 6. Such investigations should provide a better understanding of nanoparticle radiation physics applied to biomedical applications.

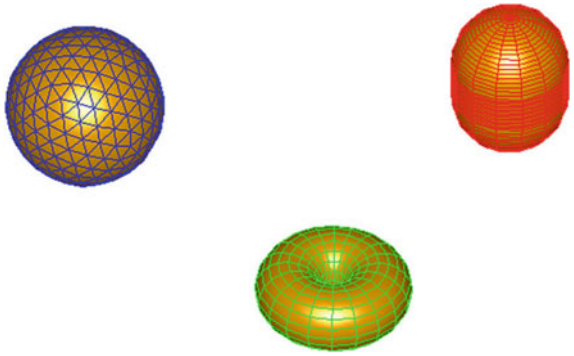

Fig. 5 Investigated geometries of NPs of equivalent volume: a sphere, a rod and a torus. The volume determined for a spherical NP of 5 nm radius is 523.6 nm^3

Fig. 6 Methodology for modelling coated and non-coated metallic nanoparticles in MNPBEM Matlab toolbox

6 Nanoparticle Toxicity

The range of biological responses induced by NPs is governed by chemical and physical properties that impact a number of important cellular processes including biocompatibility, biodistribution, toxicity and cellular uptake. Gold has gained increased attention as it exhibits good biological compatibility, low cytotoxicity and is relatively easy to synthesize. Elemental gold has been considered to be biologically inert, however, on the nanoscale, it has been shown that the surfaces of gold NPs are chemically reactive [93]. This occurs for NPs below 5 nm as they react differently with the environment and generate an electromagnetic field due to surface plasmon resonance effects [94]. This phenomenon is due to a coherent oscillation of the free electrons which generates the electromagnetic field on the surface of the gold NPs. Other metal NPs such as platinum, silver and gadolinium have also been investigated. However, they are generally more toxic to cells [3, 6, 11, 12, 14].

The biodistribution and elimination of NPs from the body is an important consideration in the context of NP toxicity. It is desirable for non-biodegradable NPs to be rapidly eliminated from the body to avoid long-term side effects. This is achieved through renal clearance which prevents accumulation in organs such as the heart and liver [18]. If the NPs are smaller than 5–6 nm in size, they are usually eliminated by renal clearance independently of their charge. These small sized NPs are excreted faster [17, 19] and are taken up less by cells [20, 23] but they present a more even distribution as they diffuse further within the tumor [20, 23]. It has been reported that NPs with a size range of 6–10 nm are cleared by the liver, particularly when positively charged. In contrast, NPs greater than 10 nm are retained by the liver [18].

Biodistribution studies of gold NPs with a DTDTPA coating (Au@DTDTPA) have revealed accumulation in the heart and liver, which has been shown to gradually decrease as the signal increases in the bladder and kidneys after 30 min. This indicates that the main elimination pathway was through renal clearance with non-specific uptake by the mononuclear phagocyte system, which is reduced due to the NPs negative charge. For Au@DTDTPA-Gd NPs, contrast enhancement for MRI was achieved in rats with low toxicity observed for a 72 h exposure, despite the known toxicity of gadolinium. These results may be attributed to chelation onto the surface coating of the AuNP [16]. These NPs start to accumulate in the kidneys 3 min after intravenous injection in mice and reach a maximum concentration in the tumor 3–7 min after injection. No accumulation in vital organs or aggregation was detected 6 weeks after injection. AGuIX NPs significantly improve image enhancement with MRI shortly after being injected into mice (1 min), and this remains constant for 24 h. Furthermore, 95 % of these NPs are excreted by renal clearance during a period of 18 days. AGuIX NPs also have very low toxicity. No visible accumulation in the healthy tissues, inflammatory processes or pathologies in the lungs were detected [95].

AuNPs toxicity can vary with the characteristics mentioned above but also differ in various cell types. For example, Pan et al. [96] showed that the toxicity of AuNPs on different types of cells, including mouse fibroblast, macrophages and HeLa cervical

cancer cells, is size-dependent but does not depend on the type of coating or the cell type [97]. However, differences in toxicity were observed in HeLa cells using AuNPs with different coatings [96, 98] Moreover, a study presented in Ref. [99] explored the toxicity of 33 nm AuNPs on three types of cells, namely on the A549 carcinoma lung cell line, the BHK21 baby hamster kidney cell line, and HepG human hepatocellular liver carcinoma cells. It was demonstrated that these NPs were toxic only in the A549 cells [99].

To explore the potential toxic effect of NPs used within the ARGENT network, different NPs have been tested in vitro using a range of different exposure times, concentrations and cell assays such as the MTT, MTS short term viability assays and clonogenic assays. The clonogenic assay gives information about the long term proliferative capacity whereas the two colorimetric assays, the MTT (3-(4, 5-dimethylthiazol-2-yl)-2, 5-diphenyltetrazolium bromide) or the MTS (3-(4, 5-dimethylthiazol-2-yl)-5-(3-carboxymethoxyphenyl)-2-(4-sulfophenyl)2H-tetrazoli-um) give information about cell metabolism.

Two ESRs Sophie Grellet and Vladimir Ivošev are working specifically on "Uptake dynamics of nanoagents and effect on radio-enhancement" and "Exploring site specificity, structure and sequence dependence of radiation-induced damage", respectively. The project of Sophie Grellet, conducted at the Open University (Milton Keynes, UK), is supervised by Jon Golding, Nigel Mason and Malgorzata Smialek-Telega at a multidisciplinary level. The project of Vladimir Ivošev is conducted at the Molecular Sciences Institute of Orsay (ISMO, France) and is supervised by Sandrine Lacombe. Another research project devoted to the nanoscale understanding of cell signalling and biological response in the presence of NPs and radiation is conducted by the ESR Soraia Rosa at the Centre for Cancer Research and Cell Biology, Queen's University Belfast under the supervision of Karl Butterworth and Kevin Prise.

7 Blood Toxicity

When NPs interact with proteins, even non-covalently, they may cause structural and conformational variations in proteins thereby inducing unexpected biological reactions and ultimately, leading to toxicity. Recent clinical studies have indicated adverse health effects of exposure to NPs through breathing. It has been evidenced that the addition of NPs may induce changes in blood viscosity and blood clotting capacity [100]. Medical use of NPs requires administration by intravenous injection. In order to design the next generation of NPs, it is necessary to measure the structure and stability of blood proteins upon interaction with NPs (see Fig. 7).

Circular dichroism (CD) is an excellent and sensitive method for rapidly evaluating the secondary structure, folding and binding properties of proteins, and recently has also been used to detect structural changes of proteins interacting with NPs. The use of synchrotron radiation (SR) to perform CD experiments (SRCD) shows several advantages with respect to the conventional CD technique. The major advantage is the high flux provided by a SR source with respect to a conventional xenon lamp

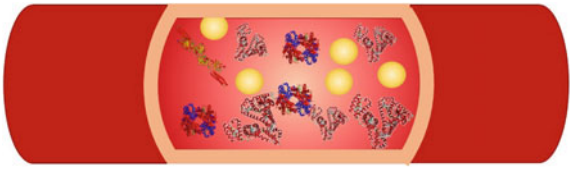

Fig. 7 Illustration of nanoparticles passing through the blood stream

that allows CD data to be measured both with very low amounts of proteins and in the presence of highly absorbing chemicals, such as suspensions of high-Z (composed of high atomic number elements) NPs [101, 102]. The high photon flux in the far-UV region, small cross section size, and highly collimated synchrotron radiation beam from the DISCO beamline at SOLEIL Synchrotron (St. Aubin, France) have allowed the group of Sandrine Lacombe at the Molecular Sciences Institute of Orsay (ISMO, France) to measure the SRCD spectra using cells with low volume capacity. The effect of Gd-based AGuIX NPs on the structure of blood proteins has been studied within the ESR research project "Improvement of the hadrontherapy protocols using nanosensitizers" carried out by Marta Bolsa Ferruz at ISMO under the supervision of Sandrine Lacombe. Human serum albumin (HSA) has been chosen for this study since it is the most abundant protein in the circulatory system and a multifunctional transporter molecule. The inactivation of HSA would lead to life threatening problems. The goal of this study is not only to assess the toxicity of AGuIX under intravenous injection but to optimize a sensitive test of NPs toxicity in blood.

8 Cell Lines

The scope of the ARGENT project is to better understand the processes of radiotherapy at the nanoscale in order to develop a new generation of radiation-based therapies able to treat different types of cancer. Towards this aim, several ESRs are performing experimental studies using a wide range of different in vitro models. In addition, the potential selective effect of NPs is explored in cancer cell models and also in appropriate normal tissue cell models. Here we detail the cell lines under investigation and the rationale for their selection.

One of the cancer types that we are focused on is prostate cancer as it corresponds to 8 % of the total of newly diagnosed cases and 15 % of the diagnosed cancers in men [103]. We are using prostate cancer cell lines, such as PC-3 and DU-145, and comparing these with normal epithelial prostate cells such as PNT2-C2. As PC-3 cells are derived from bone metastasis and DU-145 from brain metastasis, this gives us the possibility of comparing different behaviors of metastatic cells that occupy distinct microenvironments.

Astrocytoma is also a cancer of interest. The national cancer institute estimates an incidence rate of two to three per 100,000 adults per year and it represents 17 % of all

brain tumours. The life expectancy with standard treatment is about 2–3 years [104]. We are using the U87 cell line in our experiment, a model of glioblastoma multiform, which represents a high grade of astrocytoma and the most challenging brain tumor to treat [104].

Pancreas cancer follows the same tendency. The estimated incidence of pancreatic cancer is 4.1 per 100,000 adults per year. This cancer is almost always fatal. Approximately 5 % of adults in England survive 5 years after being diagnosed [104]. Indeed, it is the seventh most common cause of death from cancer. The cell line used as a model of pancreatic cancer is BxPC-3. It was derived from the pancreas of a 61 year old female patient. The morphology of this cell line is epithelial and the cells are adherent in cell culture.

Breast cancer is the leading killer among women aged 20–59 years worldwide [103] and was the cause of 521,000 deaths worldwide in 2012. For studying the effect of NPs on this cancer we used MCF-7 as a model of breast cancer and MCF-10A as its respective healthy tissue.

We are also interested in squamous carcinoma skin cancer. It is the second most common skin cancer after basal carcinoma and is also the most likely to metastasize. About 5.4 million of these two types of cancers are diagnosed each year [105]. The first line of treatment involves excision but it can also include radiotherapy [106]. In ARGENT, we use two different cell lines, the HSC-3 cancer line and the HaCaT normal skin keratinocyte line.

Cervical cancer (represented by HeLa cells) is explored in this network since it is the second most common cancer in women living in developing countries [103]. HeLa is a human adenocarcinoma cell line extracted from the cervix of 31 year old African female patient. Its morphology is epithelial and it is adherent in cell culture. It is also a good model of a radioresistant cancer. Since this cell line has been used for many decades it is well understood and can give key information on NPs response and radiosensitization.

In some experiments conducted by the ARGENT consortium, other cell lines have been utilized. For instance, the studies of NP uptake (see Sect. 9) considered also U-CH1 (human chordoma cancer) cells derived from the sacral bone of a 56 year old Caucasian male patient and primary dermal fibroblasts that are human fibroblasts derived from the foreskin of a male African new-born.

9 Gold Nanoparticle Uptake and Retention in Cancerous and Healthy Cells

Improving our knowledge about the dynamics of nanoparticles' (NPs) uptake by cancer cells and effects on radiosensitization is essential [107]. The goal of the ESR project "Uptake dynamics of nanoagents and effect on radio-enhancement" carried out by Vladimir Ivošev at the Molecular Sciences Institute of Orsay (ISMO, France) and supervised by Sandrine Lacombe is to better understand the uptake of gold

nanoparticles (AuNPs) in different human cell lines. The methods detailed in this section can measure the uptake of NPs into cells, and techniques that give insight into the mechanisms of cellular NP uptake for different cell lines are also described along with preliminary results.

To measure the cellular uptake, inductively coupled plasma mass spectrometry (ICP-MS) is one of the best quantitative techniques. In ICP-MS, the sample is ionized and passed through a magnetic field to separate and quantify the ions produced, on the basis of their charge and size. This technique can give high specificity and excellent limits of detection [93].

The uptake of NPs by cells can also be explored by transmission electron microscopy (TEM). This technique takes advantage of the high electron density of AuNPs or other high atomic number NPs. It uses electromagnetic lenses and directs high intensity beams of electrons through the samples [108]. It can give an image resolution of 1 nm. In addition, dynamic light scattering can be performed on living cells to visualize the location of AuNPs by using their elastic light scattering properties. Fluorescence microscopy can also be used on living cells to study NPs localization in specific organelles by using fluorescent probes [109] but it can also follow the NPs inside cells if a fluorophore is attached to it. All these microscopy techniques allow one to gain special information and the precise localization of NPs in cells.

Small AuNPs (<10 nm) studied in this research project were synthetized by S. Roux and collaborators [110]. These NPs are advantageous as they amplify the effects in vivo of gamma rays and can be detected by imaging. In this study, the AuNPs are coated with dithiolated diethylenetriaminepentaacetic acid (DTDTPA). For the purpose of our experiments AuNPs were tagged with an organic dye, cyanine 5.

The following cell lines have been considered: U87-MG (human glioblastoma), HeLa (human adenocarcinoma), PC-3 (human prostate cancer), BxPC-3 (human pancreatic cancer), U-CH1 (human chordoma cancer) and primary dermal human fibroblasts (see the description of different cell lines in Sect. 8). All cell lines were bought from ATCC, Manassas, Virginia, USA.

Uptake of the AuNPs in the cells was measured by flow cytometry. Two-photon fluorescence-lifetime imaging microscopy (FLIM) was used to confirm the uptake of AuNPs in cells. Finally, ICP optical emission spectroscopy (ICP-OES) was used to quantify the number of AuNPs internalized.

The first results have demonstrated that the uptake of AuNPs varies significantly between the different cancer cell lines. The internalization of NPs is often attributed to endocytosis [111]. In this work, we investigated the role of other uptake mechanisms by using various chemical inhibitors [112, 113]. These preliminary results show that the route of uptake is also cell type dependent. First results demonstrate that cell lines with low uptake levels of AuNPs are less sensitive to the inhibitors of endocytosis, which indicates that the uptake takes place by other routes and it needs to be further analyzed. Lastly, the measurement of retention times of AuNPs in cells show that the NPs tend to be stored in cancer cells (tumors) at high concentrations for more than 48 h, whilst they are efficiently excreted from primary fibroblasts (healthy tissues).

This work highlights how diverse and complex the response of cancer cells to a perturbation, such as the presence of NPs, is, and how specific treatment must be in order to be effective. More importantly, the results have shown that the NPs used for radiotherapy tend to reside longer in cancer cells compared to healthy cells, even in in vitro conditions. This fact gives NPs a promising future as radio enhancers in radiotherapy and increases the likelihood of their use in clinical conditions. However, improvements of NPs in terms of targeted tissue specificity and harmless elimination from the organism after the tumor eradication are essential for their future application in radiotherapy.

10 Particle Tracks

Understanding how the physical interaction of primary ions, photons and electrons with biological media guides dose deposition is a fundamental issue in clinical treatment planning. Indeed, the different dose deposition patterns arising from photon and ion interaction with biomaterials are responsible for their different relative biological effectiveness (RBE). While photons mainly interact with the condensed phase target by Compton scattering, producing a large number of high energy electrons, ions mainly transfer their energy to the system by glancing collisions with the target electrons, producing a large number of low-energy electrons. This fact differentiates the track structure of both radiation qualities: photons deposit dose in a quite homogeneous manner (photoelectrons generally travel large distances and experience many collisions), while the low-energy electrons ejected by ion beams experience a lower number of elastic and inelastic collisions, creating a nanometer track structure around the ion's path. As a consequence, intense radial doses are deposited around the ion's path, which produces a larger number of clustered damage events in surrounding molecules, leading to an increased RBE. Experimental quantification of radiation damage at the molecular scale is considerably more difficult than performing a predictive numerical experiment covering all the physical channels leading to energy deposition. This section presents a description of the background of particle track simulations along with a deeper discussion of the two codes used in the ARGENT project.

In fact, an essential task of medical physicists is to fit the actual dose delivered by the ion beam (or any incident radiation modality) within the patient as close as possible to the dose calculated by the computerized treatment planning system [114, 115]. Since hadron therapy (as well as conventional radiotherapy with X-rays) involves several stochastic processes due to the enormous number of collisions, dose planning is performed by computer simulations. A direct consequence of this is the development of dose calculation algorithms mostly using the Monte Carlo approach, which can be divided into two areas: radiation transport and track structure codes. While the former are more suited for macroscopic dose calculations in the whole irradiated volume, the latter are focused on a small portion of the track in order to study the particular type of dose delivery on the nanoscale, e.g., its density, which is thought to correlate with the biological efficiency. Within the ARGENT project, we preferentially select

the latter since it allows a complete understanding of the nanoscale radiation effects, including secondary species such as radicals and secondary electrons. However, it should be noted that other kinds of Monte Carlo codes, useful for specific purposes, have been discussed within this book, e.g., in the Chap. "Propagation of Swift Protons in Liquid Water and Generation of Secondary Electrons in Biomaterials" by P. de Vera, R. Garcia-Molina, and I. Abril. As examples of track structure codes, PARTRAC [116], KURBUC [117], NOTRE DAME [118], EPOTRAN [119], Geant4-DNA [120], LEPTS [121] and TRAX [122] have been designed for track structure simulations, among others [123, 124]. Within ARGENT, two track structures codes, namely LEPTS and TRAX, are being improved and undergoing validation studies for late biomedical applications. Therefore, in what follows we focus on these two modeling approaches.

LEPTS (Low Energy Particle Track Simulation) tracks the secondary electrons produced by the primary projectiles by sampling the appropriate cross section data and the corresponding energy loss spectra [121, 125]. A more detailed description of this code and its capabilities are provided in another chapter of this book (see the Chap. "Monte Carlo-Based Modeling of Secondary Particle Tracks Generated by Intermediateand Low-Energy Protons in Water" by A. Verkhovtsev, P. Arce, A. Muñoz, F. Blanco, and G. García). The total scattering cross sections are based on calculations and transmission beam experimental data and ultimately define the mean free path of the electrons, hence the spatial location of the interaction. Then the energy loss distribution, taken from experimental data, determines the amount of energy transferred. These are discussed in further detail in Sect. 13. Throughout the scattering process until thermalization the path is modified by the integral and differential elastic cross sections, both derived from measurements and calculations. Finally, Monte Carlo sampling according to the integral and differential inelastic interaction probability function drive the multiscale electron-driven processes responsible of the radiation damage [123].

The ultimate goal of the simulation procedure is to provide a full track of the primary ion (or photon or electron) and its secondaries, down to 1 eV, tracking biomolecular dissociations that occur. In order to build up a full energy deposition model, LEPTS is run jointly with classical Monte Carlo codes. For instance, Geant4 or Penelope can be used above 10 keV and LEPTS can take over below 10 keV to account for quantification of low energy physics based on reliable cross section data for ionization, electronic excitation, vibrational excitation, rotational excitation, electronic attachment and neutral dissociation [123]. These low energy scattering processes are difficult to take into account in a physical, clinical detector, and require technical expertise not yet present for medical physicists working in radiation oncology. The numerical experiment, using LEPTS, offers an excellent alternative to reach the molecular level of dosimetry for an accurate description of secondary species' (radicals and low energy electrons) interactions. The validation of the LEPTS methodology by a comparison with the outcomes of commercial treatment planning systems is the task of the ESR research project "Validation of low energy scattering model in medical radiation planning" carried out by Ali Traore at CSIC (Madrid, Spain) under the supervision of Gustavo García.

TRAX is a Monte Carlo particle track structure code developed during the last 20 years at GSI (Gesellschaft für Schwerionenforschung, Darmstadt, Germany). This code has been designed to simulate the passage of ion and electron radiation in dosimetric devices and radiation damage in biological systems. The software can, then, cover a range of radiation energies compatible with these applications: from a maximum energy of few hundred MeV/u for ions and few hundred keV for electrons to a lower threshold of between 10 and 1 eV. The lower threshold and then the accuracy of the simulations are given by the available cross sections. These cross sections can either be calculated from semi-empirical and analytical formulae or read from external cross section tables.

The ions and electron tracks are simulated considering ionization, excitation and elastic scattering interactions with the target material. The target material can be atomic or molecular or a mixture of atomic and molecular materials. Some complex materials like air or plastic are included as well. In more recent versions of TRAX, information regarding the yield of Auger electrons is included in the target characterization, and plasmon excitations for solid state material (volume plasmon) are also accounted for [126]. Thanks to the capability to follow the secondary electrons down to very low energies, the code allows the calculation of many relevant radiation quantities, such as the radial dose distribution, depth dose distribution, W-values, micro-dosimetric quantities such as the lineal and specific energy transfer, secondary electrons spectra and the ionization distribution. Recently the effect of radiosensitization of gold NPs has been also implemented in TRAX. This code, indeed, has proven to be very suitable for such applications since it can simulate the electron paths on a nanoscopic scale and can handle complex geometry, such as NPs in water solutions [127].

11 Computer Simulations of Ion-Induced Shock Waves

As explained before, one of the main characteristics of the interaction of energetic ion beams with tissue is that most of the energy is lost by ejection of low energy secondary electrons, mostly with energies around or below 50 eV around the Bragg peak region, irrespectively of the biological target considered [128–130]. The further propagation and interaction of these electrons with the biological environment can be studied by different techniques, including track-structure Monte Carlo simulation codes, as explained in Sect. 10, or analytical techniques such as the random walk approximation [128, 131].

A recent analysis of the track-structure performed within the random walk approximation revealed not only the well-known feature of the very intense and steep radial dose deposited around ion tracks, but also that this radial dose is built up very quickly, in around 50 fs [131]. As a result, a large amount of energy is deposited in very small volumes (cylinders with a radius of $\leq$1 nm), and in a time scale much shorter than the times in which the electron-phonon coupling operates, the mechanism capable of dissipating this energy. As a consequence, large amounts of energy will be deliv-

ered at once to the translational and vibrational degrees of freedom of liquid water surrounding ion tracks (what we will refer to as "the hot cylinder"), which posses the initial conditions for a violent explosion. Such observations are in agreement with previous estimates, based on the thermal spike model that suggested large increases in temperature around ion tracks in the sub-ps scale [132, 133]. Therefore, it is quite clear that the conditions for this violent explosion of "hot" nanocylinders surrounding ion tracks are plausible and may lead to the formation of cylindrical shock waves on the nanoscale.

Such ion-induced shock waves were first analyzed in terms of a classical hydrodynamics model [133]. Based on the initial conditions explained above, the hydrodynamics equations for the self-similar flow of water were solved for the cylindrical case of energy deposition around an ion track on the nanoscale. Several useful quantities characterizing the ion-induced shock waves were obtained, such as the velocity of propagation of the front and its pressure. The front velocity is proportional to the stopping power to one fourth, while the pressure of the front is directly proportional to the stopping power [133–135]. From these dependencies, it is possible to predict the main features of ion-induced shock waves, depending on the stopping power of the incident ion. The space and time scales in which shock waves operate can also be known: shock waves damp in times of about 10 ps, and they propagate in distances of a few tens of nanometers [133]. This time scale lies in between the initial propagation of secondary electrons and the further chemical effects produced by the diffusion and reaction of free radicals.

Although the main shock wave characteristics can be predicted by the hydrodynamics model, its effect on biological molecules cannot be obtained. For these purposes, it is possible to use atomistic simulations, such as the classical molecular dynamics described in Sect. 5, to predict whether the high pressures produced during the shock wave are enough to produce damage of biomolecules such as DNA. Within the ARGENT project, this analysis is being performed by the ESR Pablo de Vera under the supervision of Andrey Solov'yov (MBN Research Center, Frankfurt, Germany), Frederick Currell (Queen's University Belfast, UK) and Nigel Mason (The Open University, UK). The objective of the project is to theoretically characterize the features and effects of ion-induced shock waves, and also to provide data that can be checked experimentally, to demonstrate the existence of these shock waves.

Several works have been performed in this direction over the last few years [135–138], where, most significantly, it was shown that shock waves can deposit enough energy to produce single strand breaks (SSBs) in DNA, with probabilities, for high stopping power ions, even larger than the effect of free radicals [136].

More recently, within ARGENT, another molecular dynamics study has been performed by Pablo de Vera on the effects of ion-induced shock waves in short DNA duplexes [135]. This study showed that molecular dynamics simulations can perfectly reproduce the main wave front features predicted by the hydrodynamics model. Such results are relevant, since these characteristics are found in agreement from two different methodologies, this gives more support to the theoretical prediction of shock waves.

Final confirmation of the existence of shock waves should come from their experimental observation. Several quantities related to the effects of shock waves in DNA molecules might be observed experimentally, such as their geometrical distortion or the number of strand breaks produced. If we take into account that backbone bonds can be broken with energy deposition events $\geq$2.5 eV (as a conservative estimate), it is quite obvious that the probability of producing an SSB by carbon ions is not very large, according to the molecular dynamics simulations results. However, it is much more important for the case of heavier ions, such as iron [135, 136]. Such results for the short DNA duplex are compared with the previous results for the nucleosome. It has also been shown how heavier ions (iron) produce larger nano-channels in liquid water, as a result of the nano-cavitation effect induced by the shock waves [135]. Thus, the use of ions heavier than carbon would be more convenient for experimental evaluations.

We expect that any of the above described events (production of single strand breaks, production of nano-channels, bending/fragmentation of DNA) could be observed experimentally in the near future, and that the simulations described might help on the setting up and interpretation of potential experiments for shock wave detection. This, among other possibilities, such as the detection of the shock wave signature on the distribution of free radicals after irradiation (due to the velocities of the shock wave, much faster than diffusion) [136] are being considered within ARGENT, for a combined experimental and theoretical study of the biological effects of ion-induced shock waves. Further and more detailed explanations of all the topics discussed can be found in Chap. "Thermo-Mechanical Damage of Biomolecules Under Ion-Beam Radiation" of this book.

12 Radical Production

When describing the effect of radiation on biological media, it has to be considered that up to 70 % of the radiation damage is induced indirectly by the action of the water-derived free radicals. Water radiolysis produces highly reactive free radicals able to inflict severe damages on biological media, mostly $OH^{\cdot}$, $H^{\cdot}$, $^{\cdot}O^{\cdot}$ and e^{-}_{aq}. Among them, hydroxyl radicals ($OH^{\cdot}$) are supposed to be the most injurious as they are believed to be the main component responsible for cell killing via indirect damage [139]. Being very powerful oxidizers with high electron affinity, $OH^{\cdot}$ radicals can bond with free electrons produced during the irradiation preventing their recombination with the positive ion. In addition, two very toxic species (hydroperoxyl radical, $HO^{\cdot}_2$, and hydrogen peroxide, H_2O_2) are generated by the interaction of $OH^{\cdot}$ with water molecules from the medium and other free radicals produced during the radiolysis. In this section, the radical production, oxygen effect, influence of NPs on these and their respective timescales are articulated.

In radiation chemistry, the quantity used for describing the yield of free radical production is the G-value. This is the number of radicals produced per 100 eV of energy deposited by radiation in the medium. Experimentally this quantity can

be established with high time resolution by means of pulsed radiolysis experiments. Useful information on the impact of the indirect damage can, in addition, be obtained by performing experiments with radical scavengers. In these experiments the direct and indirect damage are disentangled by the use of chemicals able to interact with reactive species, such as free radicals, thereby blocking the indirect effect of radiation. Dimethylsulfoxide (DMSO), for example, is a scavenger commonly used to inhibit the effect of $OH^{\cdot}$ radicals. With this approach, a significant decrease of the indirect effect has been observed for high linear energy transfer (LET) radiation [140, 141]. In particular, a drastic decrease of the yield of hydroxyl radicals has been measured with the increase of the LET. This kind of behavior, also predicted from several simulation tools [117, 142–144], is supposed to be related with the track density: for high LET the track is more dense and recombination processes between radicals are more likely to happen [145].

Another important parameter, which significantly affects the impact of the indirect damage, is the oxygenation level of the irradiated material: the increasing radioresistance of hypoxic tumors seems to be strongly related with the indirect effect of radiation [146] and in particular with the yield of OH radicals [147]. This effect is generally explained as a combination of two main phenomena. On one hand, the molecular oxygen in the solution reacts with the radical species generated during the irradiation and increases the yield of production of HO_2 and H_2O_2. On the other hand, the oxygen seems to be able to fix the DNA damage caused by radicals making it permanent. Reacting with a radical, the DNA can be ionized becoming $DNA^{\cdot}$. In absence of oxygen this damage can easily be repaired and come back to its original state of DNA-H; however, if there is a molecular oxygen in the proximity, the $DNA^{\cdot}$ can react with it leading to the formation of a hydroperoxyde radical, in this case the damage is fixed and irreparable. This process is described by the following reactions:

$$\mathrm{DNA}^{\cdot} + \mathrm{O_2} \rightarrow \mathrm{DNA - O - O}^{\cdot} \quad \text{(DNA peroxide radical)}$$
$$\mathrm{DNA - O - O}^{\cdot}\mathrm{H}^{\cdot} \rightarrow \mathrm{DNA - O - OH} \quad \text{(DNA hydroperoxide).}$$

Recently a significant increase in radical production has been observed in the presence of gold and platinum NPs [148, 149]. This phenomenon seems to be related to surface effects such as a high concentration of low-energy electrons due to the surface plasmon effect [150], catalytic interaction between the metal surface and the water dipole [148], or geometrical factors like the surface/volume ratio for high-Z materials [149]. Even though this effect has still to be deeply investigated and a thorough theoretical description is not available, these observations are very promising in the context of using noble metal NPs as radiosensitizers, especially in conditions where the suppression of the indirect damage is the main cause of radioresistance, e.g., in the case of hypoxia.

Despite the high relevance of the indirect damage in the radiation effect, many theories are still not completely proven and a mechanistic description able to describe the impact of the indirect effect from different irradiation conditions is yet to be developed. At the moment only a few Monte Carlo particle track structure codes are able to describe the evolution of the track on the chemical level as well: PARTRAC [143],

CHEM-KURBUC [117], RITRACKS [142], and GEANT4-DNA [144]. In all these software the effect of radiation is represented as a three-stage process. These stages, characterized by different time scales, are identified, according to the standard paradigm of radiation damage, as: the physical stage, the pre-chemical stage and the chemical stage.

Physical stage: this lasts for the first 10^{-15} s after the irradiation. The primary particles and secondary electrons excite and ionize the water molecules. This phase corresponds to the direct effect of radiation.

Pre-chemical stage: in this stage the chemical species produced by the ionization and the dissociation of the ionized and excited water are generated. Ionized water molecules generate H_3O^+ radical ions and $OH^{\cdot}$ radicals. Excited water molecules instead have different channels of dissociation depending on the molecular excitation level. The species produced by the dissociation of excited water molecules are H_2O, $OH^{\cdot}$, $^{\cdot}O^{\cdot}$, $H^{\cdot}$, H_2, H_3O^+ and sub-excitation electrons. This stage ends with the thermalization of all the chemical species around 10^{-12} s after the irradiation.

Chemical stage: includes the Brownian diffusion and the reactions between all the chemical species generated during the pre-chemical stage. During this phase the track evolution is generally described by a step by step approach. During each time step, t, the radicals diffuse randomly with a step size dependent on their diffusion coefficient, D; the distance traveled, l, is sampled by a Gaussian distribution with a root mean square calculated according to the Smoluchowski diffusion equation: $\langle l \rangle = \sqrt{6Dt}$. The reactions between radicals are instead defined via a proximity parameter generally indicated as the reaction radius, a: two radicals interact if their separation is smaller than $2a$. The definition of the reaction radius changes depending on if the reactions are assumed to be diffusion controlled (as in CHEM-KURBUC), partially diffusion controlled (as in PARTRAC) or if more complex models are taken into account (as in RITRACKS). The chemical stage lasts up to 10^{-6} s; after that time the chemical development of the track is supposed to be over and the radical yields are assumed to be constant.

Within the ARGENT project, the action of water-derived free radicals is investigated, theoretically and experimentally, under different irradiation and oxygenation conditions. This is the main task of the ESR research project "OER prediction on the nanoscale for a target tissue in different conditions of irradiation and oxygenation" carried out by Daria Boscolo at GSI (Darmstadt, Germany) under the supervision of Emanuele Scifoni and Marco Durante. For this purpose a chemical extension of TRAX is currently under development and experiments in collaboration within the ESR project of Marta Bolsa Ferruz, "Improvement of the hadrontherapy protocols using nanosensitizers" are currently ongoing (see Sect. 16).

13 Collision-Induced Processes

The in-depth understanding and ongoing research described above for the production of secondary species, be they electrons or radicals, ions and neutrals, are vitally important for understanding the total impact of radiation on living tissue. The cas-

cade of low-energy (<5000 eV) particles produced in photon and ion radiotherapy, with and without the presence of nanoparticles, is capable of inducing irreparable damage in living cells through a range of low-energy physical processes [151–154]. A full understanding and control of nanodosimetry, the effect of the radiation dose in nanovolumes in the cell, plays an important role in the effectiveness of radiotherapy modeling [155]. This is the major work of the ESR Lilian Ellis-Gibbings, a physicist working under Gustavo García in the Institute of Fundamental Physics, Consejo Superior de Investigaciones Científicas in Madrid, Spain. This section describes experimental and theoretical methods for the production of statistical data relating to the effects of secondary species of irradiation (electrons and anions) on biomolecules and water.

The channels these low energy secondary particles follow for their physical distribution and damage to important biological molecules include elastic scattering, rotational, vibrational and electronic excitations, as well as electron attachment and ionization. Appropriate modeling of these interactions within particle tracks is commonly and effectively undertaken using Monte Carlo codes [156], which require precise and accurate cross sections of interaction on both the medium and the molecules of interest [157]. This data, primarily in the form of total, differential (in angle and energy) and integral cross sections, along with the energy loss spectra, can be determined experimentally and theoretically. The theoretical methods have varied accuracy under different physical energy regimes [158, 159].

Electrons make up the bulk of secondary particles from photon and ion irradiation, and the majority of them are produced with less than 50 eV [160]—as such the interactions described above are possible before the electron thermalizes [151]. Since these electrons are clearly able to impact and damage biological material, part of this study is in the experimental and theoretical determination of the interaction types and cross sections for the collisions of low energy (0–5000 eV) electrons with molecules of biological importance.

Theoretical calculations of electron–molecule (and positron–molecule) impact collisional cross sections follow several main themes. Ab initio calculations are highly accurate and methods based on the close-coupling expansion, such as the R-matrix, the Kohn variational principle, and the Schwinger variational principle are popular amongst these [158, 161]. Unfortunately they are computationally expensive and inappropriate for complex molecules at intermediate to high energies [162]. In order to produce the cross sections necessary for radiotherapy particle track simulations (see Sect. 10), approximate methods have been developed. A popular starting point is the Independent Atom Model (IAM), which has proved fruitful due to its accuracy above approximately 100 eV and the ease of calculation. The IAM postulates that the scattering cross section of a molecule can be substituted with the scattering cross sections of each of the atoms in their respective positions within the molecule. It assumes each atom scatters independently, there is no multiple scattering within the molecule, and the molecular orbitals of electrons are ignored [163]. This simplification breaks down at low energies, where interference and multiple scattering begin to have an effect.

Equation (2) describes the basic additivity rule (AR) of the IAM for any molecule, derived through application of the optical theorem, where σ denotes a cross section. The first modification of this approximation is a correction to the additivity rule—based on the fact that at lower incident energies, scattering cross sections become much larger to the point of overlapping—so to sum them completely effectively counts some areas twice and hence overestimates the calculated molecular cross section [164, 165].

$$\sigma^{\text{molecule}} = \sum_{\text{atoms}} \sigma^{\text{atoms}}. \tag{2}$$

Equation (3) describes the Screening Corrected Additivity Rule, where s_i is the screening coefficient dependent upon the cross section of the other atoms in the molecule, and α_{ij} a term that gives the overlap of the cross sections within the molecule. This treatment managed to bring the accuracy of the IAM method down to 6 eV for C_3F_2 and has since been used in the >10 eV incident energy range, for total and differential elastic and inelastic cross sections. The differential cross section is treated with a redispersion factor described in detail elsewhere [165] which deals with the shielding of waves both into and out of the molecule. Multiple scattering events are included [159, 162] and are shown to be necessary between 1–300 eV incident electron energy.

$$\sigma^{\text{molecule}} = \sum_i s_i \sigma_i \qquad s_i = 1 - \frac{1}{2} \sum_{j \neq i} \frac{\sigma_j}{\alpha_{ij}}. \tag{3}$$

These improvements in the calculations for cross sections of low energy electron-molecule collisions are verified by experiment and ab initio calculations, and both experimental and calculated values are used as data tables in particle track simulations. Experiments also provide information on electron energy loss spectra and fragmentation pathways that are difficult to ascertain using approximations as simple as the IAM. Experimental criteria include low energy spread, simplistic experimental setups to enable appropriate analysis, and close approximation to the physical reality.

Within our group, total cross sections and electron energy loss spectra for collisions of electrons with various biomolecules in the gas phase can be collected for incident electron energies between 80 and 5000 eV. These are collected using a transmission experiment shown in Fig. 8. The total cross section is the probability of any interaction between the incoming particle and the target molecule—in the transmission experiment described this is defined using the Beer-Lambert law by measuring the drop in intensity of the incident beam of electrons as a function of the gas pressure in the scattering chamber. These values are used in simulations to define how many of the electrons at each energy will interact with their surroundings. Electron energy loss spectra are primarily used for identifying the excitation resonances and ionization energy of the target molecules (Fig. 9). They are recorded in the same transmission experiment as the total cross section, see Fig. 8. The characteristic energies and relative probabilities of a molecule to undergo electronic excitation, ion-

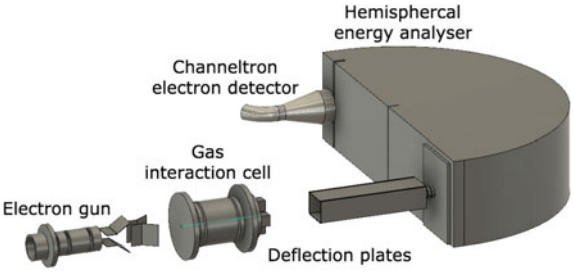

Fig. 8 Apparatus for both total cross sections and energy loss spectra, located in Madrid, Spain. Electrons from the electron gun cross biomolecules in the interaction chamber, and are analyzed by energy in a hemispherical analyzer and channeltron

Fig. 9 Electron-molecule collisions result in various energy loss processes for the initial electron. As an example here you can see clearly the electronic excitation peak in pyrimidine of the $^1A_1$, $^1B_2$ $\pi \rightarrow \pi^*$ transitions at 7.6 eV. The initial energy of the impacting electron is shown in the legend. The figure is adapted from Ref. [166]

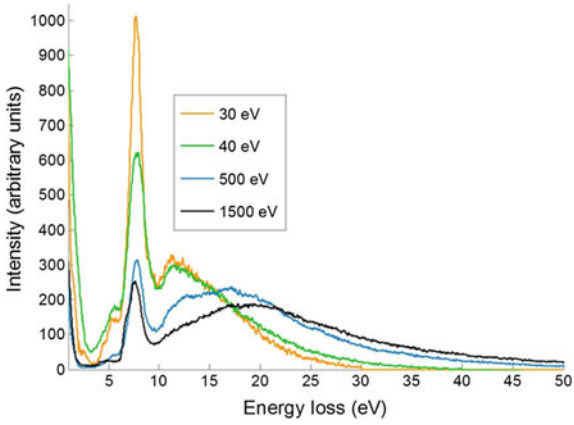

ization and autoionization following excitation are all clear in the spectra. With some deconvolution it is also possible to determine detail about the vibrational excitation and highest energy inner shell ionization.

Through their interactions with the medium, electrons, like the incident therapeutic radiation, are capable of ionizing molecules and creating radical species such as negative ions. As mentioned, these species are an immensely important part of radiation damage. Reactive oxygen species, such as the superoxide radical O_2^-, are particularly important in DNA damage and have been studied in biological experiments to prove their potential. As yet, no experimental cross sections of low energy anion–biomolecule collisions are available, despite their importance to radiotherapy. The following experimental setup is designed to bridge this gap.

A technique for investigating collisions of low-energy (<400 eV) negative ions with neutral biomolecules is being developed to provide details of fragmentation pathways through detection of positive, negative and neutral fragments [167]. The experiment shown schematically in Fig. 10 consists of a pulsed hollow cathode discharge, whereby the negative ions are formed in the plasma afterglow by electron attachment. The electron temperature in a hollow cathode discharge is typically

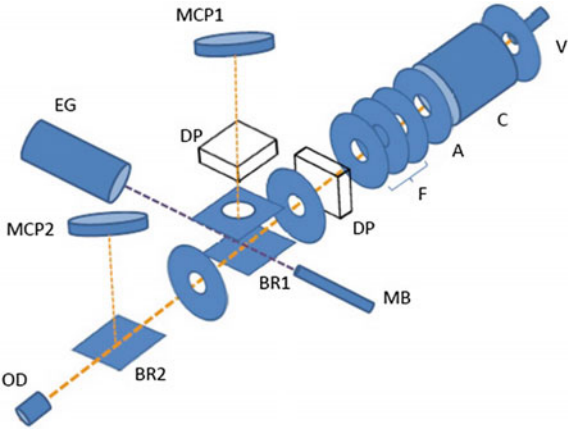

Fig. 10 Schematics of the experimental setup. *V*, pulsed supersonic valve; *C*, hollow cathode discharge; *A*, anode; *F*, focusing lens; *DP*, deflecting plates; *BR*, beam reflector; *MB*, effusive molecular beam; *MCP*, multi-channel plate detector; *EG*, electron gun; *OD*, optical detector. The figure is adapted from Ref. [167]

<10 eV, and it is well known that the electron attachment cross sections for small molecules have resonances in this range, with excited species also having enhanced attachment cross sections at resonant energies [168–170]. Once formed, the negative ion beam is guided using electrostatic ion optics to the interaction region where it crosses with an effusive beam of a biomolecular gas. Negative ions can act as electron donors for electron attachment [171], and the presence of the neutral species following this can serve to stabilize the new anion. This charge transfer leads to the formation of a transient negative ion in the target, which can subsequently autoionize or fragment as a relaxation pathway from this energetically unstable state. The fragmentation products of these processes are analyzed using time of flight mass spectrometry (TOF-MS), including the neutral fragments, which are investigated with an electron gun.

All of these interactions contribute to the biological dose, and they occur at much lower energies than the incident radiation. Their contributions are slowly being uncovered and tabulated, implemented in particle track modeling, giving direction for radiosensitization, and slowly added to clinical radiotherapy software to increase the accuracy of life saving treatment. With strong data from experiment and calculations we are able to improve our modeling far beyond the initial particle in radiotherapy, to the end goal of modeling the survival of cell lines under different conditions with different radiosensitizers.

14 Experimental Study of Electron Emission from Ion-Irradiated Metallic Nanoparticles

As mentioned above, one highly promising idea in the field of nanotechnology enhanced radiation therapy is the administration of high-Z metal-based nanoparticles (NPs) composed, for instance, of gold, platinum, or gadolinium, as potential

radiosensitizers during treatment. Their therapeutic effects are proven on the cellular level by irradiation of cell cultures and observation of the corresponding survival curves [172]. However, the full explanation of their radiosensitive properties on the fundamental level is yet to be determined. It has been associated with mechanisms that appear on different time scales, among which one of the most important is the emission of secondary low energy electrons induced by radiation and the catalytic (redox) properties due to the high surface/volume ratio that can enhance the production of the reactive oxygen species in the cellular environment [15].

In this context, it is important to determine the number of electrons which are emitted during the interaction of a specific ion with the NP. This value depends on the ion charge and velocity, the material of the NP, its size and its molecular coating as well as on the chemical environment in which the collision takes place. A theoretical approach is difficult to perform due to the large size of the radio-sensitizing system. As such the experimental approach is a promising alternative, while also representing a great challenge. Such an approach is realized in the framework of the activity of the AMA Group in the CIMAP Laboratory in Caen, France within the ARGENT project. This work is undertaken by Arkadiusz Mika under the supervision of Bernd Huber in the ESR project "Molecular efficiency of radiosensitizers in ion-induced radiation damage processes". The main goal is to construct and develop the experimental setup where under high vacuum conditions ($<10^{-8}$ mbar) a molecular beam of NPs will collide with highly charged ions and the resulting products (charged molecular fragments and electrons) will be detected. This experiment is under development, and preliminary experiments with ion irradiation of thin gold foils [173], as well as the irradiation of gold NPs by X-rays [174] have been performed.

14.1 Development of the Experimental Setup

14.1.1 Production of Nanoparticles

In order to perform a systematic study of the electron emission occurring in collisions of ions with various nanoscale targets, the first step is to create well-defined molecular beams containing biomolecules (e.g., nucleobases) in their natural cell environment (nano-solvated) with/without the presence of radiosensitizing agents or metallic clusters. This experimental approach is based on the use of a magnetron gas-aggregation cluster source [175]. Such a device is composed of 2 main elements—the condensation chamber cooled to liquid nitrogen temperatures and the magnetron head carrying the metallic target, for example a gold disk (see Fig. 11). A magnetic field-assisted discharge is ignited by a voltage of about 300 V in an argon atmosphere ($\sim$1 mbar). As the metallic target serves as the cathode, Ar^+ ions are accelerated in the $E \times B$ field towards the metal surface, forming a metal vapor via sputtering. The formation of clusters occurs outside of the discharge in the cooled condensation region.

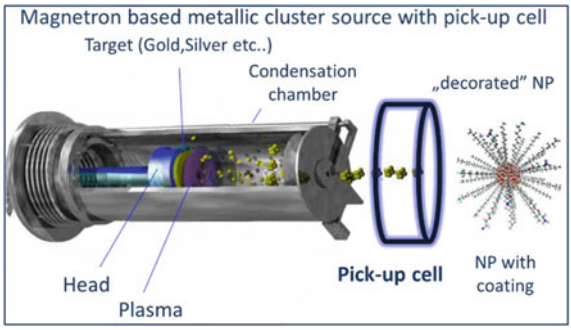

Fig. 11 A schematic view of the magnetron based gas aggregation cluster source with pick-up cell. The drawing of a NP was made by Kaspar Haume

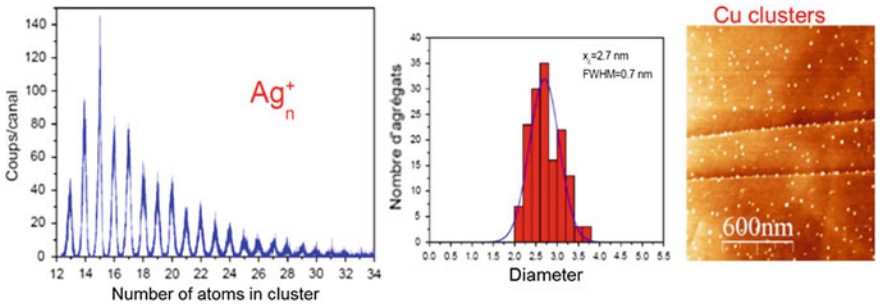

Fig. 12 Mass spectrum of small (a few atoms) silver clusters (*left panel*), the size distribution of size selected copper clusters (*middle panel*) and their deposition on a HOPG surface (*right panel*). The figure is adapted from Ref. [176]

The metallic clusters can be neutral or positively/negatively charged. After leaving the source they pass through a skimmer into a low pressure chamber where they traverse through a so called pick-up cell (Fig. 11). Here the molecular environment around the NP can be formed by the attachment of water molecules or evaporated (bio)molecules.

The thermodynamic conditions inside the source strongly influence the size and intensity of the produced NPs. These depend on the number of collisions in the aggregation source and, therefore, can be varied and controlled using the buffer gas pressure and the position of the magnetron head. For example, the formation of larger clusters is favored when the condensation length is longer. Some typical results [176] obtained with this source are given in Fig. 12. The left part shows the mass distribution of small positive, singly charged silver clusters containing between 10 and 30 atoms. In the middle part of Fig. 12, the size distribution of larger singly charged Cu^{n+} clusters is shown corresponding to particle diameters of $\sim$3 nm. The right part demonstrates the homogeneity of Cu clusters deposited on a clean highly oriented pyrolytic graphite (HOPG) surface, immobilized onto defects induced by prior ion bombardment.

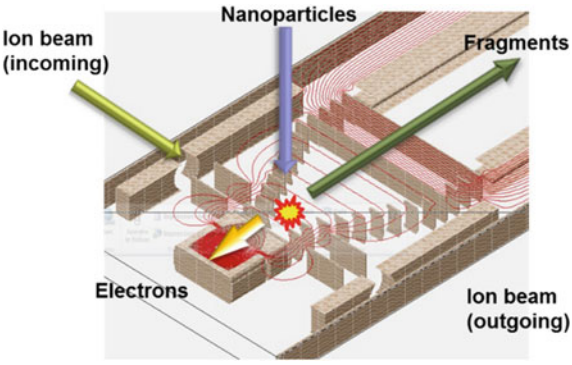

Fig. 13 The geometry of the extraction region with arrows showing the directions of the beams and products before and after the collision

14.1.2 Multicoincident Detection of Molecular Fragments and of the Number of Emitted Electrons

Extraction region: A technological challenge is represented by the coincident detection and separation of the collision products, either in the form of positive molecular fragments or the number of free electrons. For this purpose the ion extraction region (Fig. 13) was designed to be coupled with an electron statistics counter. Simulations using the SIMION software have been performed to optimize the electric fields and particle trajectories. The positively charged fragments are extracted along one direction (perpendicular to the axis of molecular beam and ion beam) into the Wiley McLaren Time-of-Flight Mass Spectrometer, whereas electrons are extracted in the opposite direction to a Passivated Implanted Planar Silicon (PIPS) detector that is kept at a high potential (more than +20 kV).

14.1.3 Electron Detection—PIPS Detector

One of the most challenging tasks is the detection of the signal coming from just one emitted electron (of the order of 0.4 mV) and a successful decoupling of this signal from the high voltage potential. As the PIPS detector and the connected electronics (pre-amplification and amplification stage) operate at a high potential, it is necessary to use an optical fiber data link to successfully decouple the energy and time signal for the multicoincidence hardware (FASTER developed at LPC Caen).

The collision process between low energy projectile ions (P) and the NP target (T) is described by the equation:

$$P^{n+} + T \rightarrow P^{(n-s)+} + T^{m+} + (m-s)e^{-}. \tag{4}$$

Here P^{n+} is a projectile with charge $n+$, T^{m+} stands for the target with charge m, s is the number of electrons stabilized at the projectile and $(m-s)$ is the number of emitted electrons. The last remaining element to provide full information about the

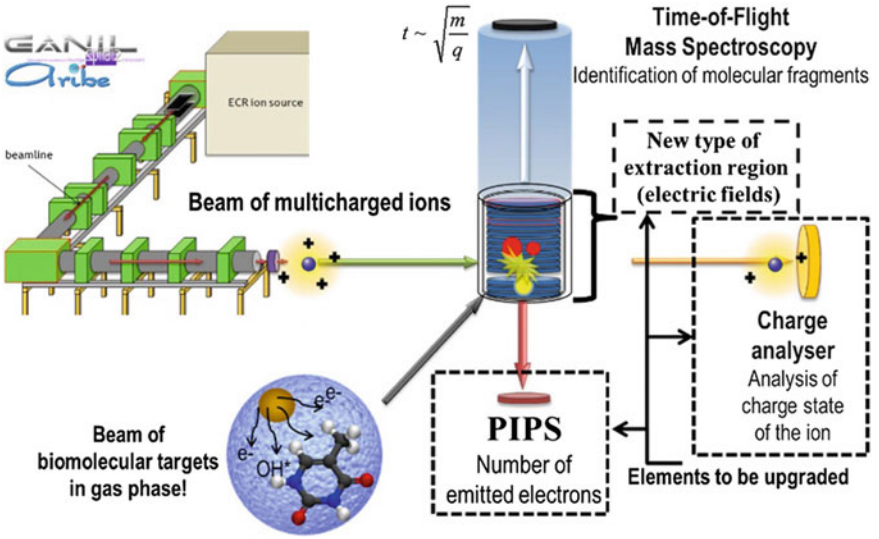

Fig. 14 Scheme of the experimental setup currently being developed for multicoincidence measurements between emitted electrons, molecular fragments and the projectile charge state after ion-nanoparticle collisions

collision process is the detection of the charge state of the projectile after collision. This will allow determination of the initial charge state of the mostly fragmented multiply charged target. In the experiment, this will be realized by the installation of a PSD type detector and the deflection of the charged projectiles after the collision with an electrostatic field.

The overall schematics presenting all elements of the experimental setup capable of characterizing the efficiency of radiosensitizing agents at the molecular level is shown on Fig. 14.

15 Impact of Nanoscale Processes and Nanoagents on Biodamage Complexity

Even though both x-rays and ion beams are ionizing radiation, and in both of them secondary electrons, free radicals, and other reactive species do the major damage to the cells, the qualitative features such as the dose dependence of the probability of cell survival are quite different for low- and high- linear energy transfer (LET) radiation [128, 177, 178]. The complexity of biodamage, which is an important distinction between the actions of high and low LET radiation, reduces the chances of damage repair and thus strongly affects the relative biological effectiveness (RBE) of ionizing radiation. This quantity is defined as the ratio of the dose delivered by

photons to that delivered by different radiation modalities (e.g., electrons, protons, or heavier ions) leading to the same biological effect, such as the probability of an irradiated cell inactivation. Determining the impact of nanoscale processes and nanoagents on RBE is also one of the goals of the ESR research project carried out by Alexey Verkhovtsev at CSIC (Madrid, Spain) and MBN Research Center (Frankfurt am Main, Germany) under the supervision of Gustavo García (CSIC) and Andrey Solov'yov (MBN-RC). This project aims to improve the understanding of the physicochemical processes initiated by the interaction of various forms of ionizing radiation with biological matter.

A nanoscale understanding of radiotherapy requires evaluation of the effects of dose deposition on the nanoscale, i.e., nanodosimetry. The research conducted within this ESR project should give new physical and chemical insights necessary for developing a nanoscale model of radiation nanodosimetry. This concept aims at a detailed description of the interaction processes occurring in nanometer-size volumes of the medium and of implications of these processes in terms of radiation damage, such as the number of ionization or dissociative events, type of generated secondary species, etc. For that purpose, deep knowledge of numerous interactions induced by charged particles traversing living matter is strongly essential and can be obtained, for example, by means of Monte Carlo track-structure simulations (see Sect. 10). This approach is discussed in more details in the Chap. "Monte Carlo-Based Modeling of Secondary Particle Tracks Generated by Intermediateand Low-Energy Protons in Water" of this book.

This research project aims to quantify the effects of the presence of nanoagents on the complexity of biodamage—damage of biomolecules, such as DNA, leading to tumor cell death. Up to this date, particular attention has been paid to the assessment of direct and indirect damage of living cells as a function of LET and has been performed within the MultiScale Approach (MSA) to the physics of radiation damage with ions (see Ref. [128] and references therein). It has been demonstrated that the phenomenon-based MSA is capable of making quantitative predictions of macroscopic biological effects caused by ion radiation on the basis of physical and chemical effects related to the ion-medium interactions on a nanometer scale. Using this approach, evaluation of the survival probability for different cell lines has been performed. We applied the MSA to describe numerous experiments, where survival curves were obtained for different mammalian cell lines under various irradiation conditions. The details of this analysis are described in the Chap. "Predictive Assessment of Biological Damage Due to Ion Beams" of this book. The advantages of the MSA allow one to extend it to many other cell lines, including radiosensitive and radioresistive cells, different cell phases, irradiation conditions (e.g., in the presence of radiosensitizers) and make predictive evaluation of radiobiological effects.

Future research in this direction should include the effects due to radiosensitizing NPs. Recently we completed the first step in this direction by performing a theoretical and numerical analysis of secondary electron production by small metallic NP irradiated by fast ions [90, 179]. Nanometer-size NPs composed of gold, platinum, silver and gadolinium, which are of current interest for application in cancer treatments for reasons discussed above, have been considered. With this analysis, we

provided a physical explanation for enhancement of the low-energy electron production by sensitizing metallic NPs irradiated with fast ions. It has been demonstrated that metal NPs significantly enhance the electron yield due to the collective response to an external electric field of a charged projectile. The role of collective electron excitations in the formation of secondary electron spectra in metal clusters and NPs is discussed in greater detail in the Chap. "Irradiation-Induced Processes with Atomic Clusters and Nanoparticles" of this book.

16 Radiation Experiments with Radiosensitizing Nanoparticles

Metallic nanoparticles (NPs) have been proposed as enhancers of radiation treatments in cancer therapy. Their high atomic number gives them higher mass energy absorption coefficients than soft tissue. Functionalized NPs can target cancer cells which allows more selectivity of the dose deposition within the tumor whilst sparing the surrounding healthy tissue. The use of NPs for radiosensitization was first demonstrated by Hainfeld et al. [10] using 1.9 nm gold nanoparticles (AuNPs) delivered systemically, prior to irradiation, in mice exhibiting EMT-6 mammary carcinomas. The authors reported a 1 year survival of 86 % in animals treated under these conditions compared with only 20 % in those irradiated without AuNPs injection. The functionalization of NPs provides further benefit in the clinical setting by increasing contrast properties in radiological imaging and MRI.

In vitro experiments have shown the potential of the gadolinium-based AGuIX NPs to amplify radiation-effects under X-ray irradiation in the keV and MeV range. The efficiency of AGuIX has also been demonstrated in vivo. The median survival time in mice was 112 days when combining AGuIX with radiation compared to 77 days for the radiation only treatment [19]. Gadolinium compounds can be used as theranostic agents due to their magnetic properties leading to improved MRI contrast. This would allow monitoring of the NPs within the tumor, providing a more precise definition of the uptake and biodistribution within the tumor. Another possibility is to attach gadolinium to metallic NPs, e.g., composed of gold. When using Au@DTDTPA-Gd NPs (see Sect. 2), it is possible to obtain the same biological effect in prostate cancer cells under gamma irradiation using half of the radiation dose [18, 43]. An improvement of the efficiency of heavy ion radiation using AGuIX NPs was observed for the first time by Porcel et al. [15]. This has opened the perspective of using theranostics approaches in hadrontherapy. An enhancement of 18.5 % and 11.3 % for carbon and helium ions respectively, was demonstrated in mammalian cells [15].

The efficacy of platinum NPs (PtNPs) to amplify ionizing radiation was quantified using plasmid DNA as a nanobiodamage probe [3]. When metallic compounds are added, additional ionizations take place due to the high ionization cross section of high-Z atoms. Incident ionizing particles and secondary electrons produced along the

track may excite inner and outer electron energy shells of the metal atom. The ionizations in inner shells in particular are followed by Auger de-excitations processes, which result in an amplification of the electron emission by the metal. The presence of high-Z atoms in the medium locally amplifies the density of ionization and the dose deposition. When DNA is loaded with platinum, Auger electrons may either interact with the DNA directly and induce stand breaks or interact with surrounding water molecules to produce clusters of radicals that may further damage DNA. The role of free radicals and reactive oxygen species (ROS) has been investigated by adding dimethyl sulfoxide (DMSO) radical scavenger. In the case of pure DNA as well as in DNA loaded with platinum compounds, the induction of single and double strand breaks (SSBs and DSBs) was strongly reduced [3]. This result confirmed that the induction of DNA damage and the amplification of radiation effects due to the metal are mostly related to the production of water radicals close to the NP [180].

On a cellular level, the interaction between NPs and the ionizing radiation produces photons and electrons [181]. The interaction of these particles with water and oxygen yields ROS that will alter the activity of biomolecules in the vicinity of the radiosensitizers. In vitro experiments have shown an increase of the cell surviving fraction when adding DMSO [147, 182]. The different studies mentioned previously confirmed that the amplification of radiation effects due to metallic NPs are mostly related to the production of water radicals close to the metal. Furthermore, the level of oxygen in cells plays an important role in ROS production and therefore in cell killing (see Sect. 12).

The precise mechanism of how the NPs act as radio-enhancers and the crucial NP characteristics required to improve this effect remain unclear. Within the ARGENT project, a set of radiation experiments on cell and animal models is planned in order to further understand mechanisms to amplify radiation-induced cell killings. The radiochemical mechanisms involved in this effect will be studied as well as the increase of radio sensitivity of cells at low levels of oxygenation. To achieve this, different LET radiation and ions are being combined with diverse NPs, such as gold, gadolinium and platinum.

This section details the various necessary modes of experimentation and preclinical trials to be undertaken by the ARGENT group, using both photon and ion radiation in vitro and in vivo and the analysis techniques undertaken by the researchers involved.

16.1 In Vitro Studies Under Photon Radiation

Different types of AuNPs are investigated in combination with radiotherapy within ARGENT. The first types of AuNPs, with an average size of 5 nm, are used with different coatings to explore their toxicity and biocompatibility potential, in combination with radiotherapy. The second type of NPs tested, also with an average of 5 nm, are provided by the ARGENT industrial partners (see Sect. 2). These NPs are composed of gold and gadolinium (Au@DTDTPA, Au@DTDTPA-Gd and AGuIX), and

their properties of amplifying the effects of photon and ion beam irradiation have been explored above. Given their theranostic properties, good biocompatility and low toxicity [18, 19, 43] they will be further characterized and tested regarding other cancer cell lines and other radiation sources.

Kilovoltage and Megavoltage X-ray radiation ranges have been shown different effects when interacting with NPs [183, 184]. The photoelectric effect is predominant at the kilovoltage range of energy and is responsible for a high photon absorption by the NPs [183]. Therefore, the radiosensitization effect of AuNPs has been mainly explored using kilovoltage photon energies. Although this energy is still used for brachytherapy treatment, Megavoltage X-rays are the main approach used to achieve an adequate dose deposition to deep tumors [185]. Despite the fact that theoretical models generally predict a lower radiosensitization effect of NPs in combination with MeV X-rays [181, 183], several groups have reported an enhancement with MeV irradiation when using gold NPs [4, 183, 184]. Therefore, a collaborative study between different laboratories within the network is exploring these two radiation energy ranges to better characterize the NPs in use. Experiments using kV and MV X-ray radiation are being performed at Northampton Hospital and Linford Wood Genesis Care Medical Centre (Milton Keynes, UK), conducted by the research team from the Open University, and also at the Centre for Cancer Research and Cell Biology in Queen's University and the Northern Ireland Cancer Centre (Belfast, UK), conducted by the research team from the Queen's University. In addition, a comparison within the ARGENT network between theoretical predictions and experimental results on AuNPs radiosensitization with X-rays of different energies will allow us a better understanding of this effect.

16.2 In Vivo Experiments Under Photon Radiation

Moving towards translational research, our studies need to focus in vitro initially and then in vivo. Our experimental in vitro results will allow us to determine the best radiosensitization conditions for each cell line and NP type. As these conditions are established, providing significant radiosensitizing results with minimal toxicity, in vivo experiments will be undertaken in the Centre for Cancer Research and Cell Biology (Belfast, UK) to validate these findings. These experiments will not only allow the evaluation of the radiosensitizing capacity of the NPs in a tumor microenvironment, but they will also assess the imaging potential to fully characterize the theranostic potential. Within this project it will be possible to make a comparative study involving gold, gadolinium and combinations of these regarding their theranostic properties.

16.3 In Vitro Experiments with Heavy Ion Radiation

As mentioned above, the low oxygen level in tumor cells is responsible for the decrease of radiosensitivity of solid tumors. Heavy ion radiation has been positioned as a possible solution to eradicate hypoxic tumors. When the therapeutic effects of ions are compared with those of photon radiation, the ions have the advantages of a large RBE [140, 186] and a small oxygen enhancement ratio (OER) [187, 188] due to the increasing ionization density and high LET. Clinical studies show that the large RBE and the small OER of ions are responsible for enhanced biological effects and improved response in overcoming hypoxia-induced radioresistance [189, 190]. A few studies have been reported on the LET dependence of OER [191]. The objective is to evaluate OER for different ions and LETs, including carbon, helium and oxygen, in the presence and the absence of diverse NPs such as gold and platinum. Since the OER may also depend on other characteristics of the beam quality, such as the dose rate, the existing techniques to shape beam distribution on the tumor will be tested: passive beam at the Heavy Ion Medical Accelerator in Chiba (HIMAC, Japan) and active beam at the Heidelberg Ion Therapy Center (HIT, Germany). These radiation experiments will be conducted by the research team from the University of Paris-Sud. The theoretical study of the OER will be done in collaboration with the GSI research team (see Sect. 12).

It has been demonstrated that the contribution of indirect damage to cell killing decreased with increasing LET. Nevertheless, indirect action still played a significant role in cell killing and contributed around 30 % to cell killing even at an LET of 2106 keV/μm [140]. A thorough study of the indirect contribution of ROS in hypoxia when NPs are present and how it varies regarding the nature and the quality of the beam is planned. NPs open the possibility of increasing cell killing in hypoxic radioresistance cells.

16.4 Analysis

For the data analysis of both photon and ion beam experiments, we mainly use clonogenic assays. These quantify reproductive cell death after treatment with ionizing radiation, but can also be used to determine the effectiveness of other cytotoxic agents. The survival fraction (SF) of cells is plotted versus the dose and the result can be modeled, for instance, by the linear-quadratic law, $\mathrm{SF}(D) = e^{-(\alpha D+\beta D^2)}$. The coefficient α corresponds to the contribution of lesions, which are directly lethal for the cell, whereas β is attributed to the contribution of additive sub-lethal lesions. The efficiency of NPs to amplify radiation-induced cell deaths can be quantified by calculating the enhancing factor, $\mathrm{EF} = (D^{10}_{\mathrm{control}} - D^{10}_{\mathrm{NPs}})/D^{10}_{\mathrm{control}}$. Here, D^{10} represents the radiation dose used to reach 10 % of cell survival in the control ($D^{10}_{\mathrm{control}}$) and in cells loaded with NPs (D^{10}_{NPs}). The dose at 50 % of cell survival is also used for comparison of the EF depending on the nature of the radiation.

Alongside clonogenic assays DNA damage is an important readout of biological efficacy. Radiation itself is known to induce DNA DSBs which can be imaged using immunofluorescent staining to quantify the number of foci present in each sample. An increased number of foci is associated with radiation exposure and directly related to cell death [192]. One of the potential radiosensitizing mechanisms of action of NPs could be due to an increase in DNA damage post-irradiation or interference with the repair mechanisms of the cell. An indication of such consequences can be identified by looking at early (1h post-irradiation) and late (24h post-irradiation) DNA damage. After only 1 h of being exposed to radiation, cells present increased foci numbers. However after 24 h these have been reduced due to repair mechanisms. If NPs are present, they can potentially increase the initial yields of DNA damage. Moreover, if there are differences after being exposed to radiation in the presence of NPs compared to the controls at 24 h this may indicate that there is interference in the repair mechanism. Thus, analyzing DNA damage could further lead to a better understanding of NPs' radiosensitizing mechanism by providing clues towards how they affect cells.

The comparison between different radiation sources, beam types, NPs and cell lines will allow us to define optimal treatment protocols that are able to improve tumor cure whilst decreasing the side effects on healthy tissue. Moreover, the theranostic potential of these NPs will be exploited to combine both diagnostic and treatment possibilities while maintaining the same therapeutic effect. These should improve the therapeutic outcome and benefit the patient's life after treatment.

17 Conclusions

As has been shown throughout this chapter, the current status of nanoparticle assisted medicine and in particular enhancement of radiation (photon and ion) for cancer therapy is improved in a big way by interdisciplinary studies and collaboration amongst research leaders in their respective fields. From the beginning, expertise is required in understanding the synthesis and effects of different nanoparticle properties on not just the cancer cells, but the entire organism, and then to go further and fundamentally control those effects. The nanoparticles show high cell specificity, complex uptake dynamics, and their effect is highly dependent on their surface coatings, shape, size and target cell type. Their interaction with radiation in biological material is being investigated along with a deepening understanding of the initial and secondary effects of ion and photon irradiation, along with the cellular and systematic effects of these combination therapies in high and low oxygen environments. All of the areas of research described here are in a perpetual feedback loop, generating direction and improvements back and forth from simulation and experiment to provide the best possible environment for a full understanding of the essentially human problem of advanced cancer treatment. The ARGENT ITN is dedicated to advancing this vast and growing field, and expects to see large scale introduction of nanomedicine to society over the coming decades.

Acknowledgements The authors acknowledge financial support from the European Union's FP7 People Program (Marie Curie Actions) within the Initial Training Network No. 608163 "ARGENT".

References

1. COST Action Nano-IBCT. http://mbnresearch.com/project-nanoibct
2. Peer D et al (2007) Nanocarriers as an emerging platform for cancer therapy. Nat Nanotechnol 2:751–760
3. Porcel E et al (2010) Platinum nanoparticles: a promising material for future cancer therapy? Nanotechnology 21:085103
4. McMahon SJ et al (2011) Biological consequences of nanoscale energy deposition near irradiated heavy atom nanoparticles. Sci Rep 1:18
5. Hainfeld JF, Dilmanian FA, Slatkin DN, Smilowitz HM (2008) Radiotherapy enhancement with gold nanoparticles. J Pharm Pharmacol 60:977–985
6. Kwatra D, Venugopal A, Anant S (2013) Nanoparticles in radiation therapy: a summary of various approaches to enhance radiosensitization in cancer. Transl Cancer Res 2:330–342
7. Malam Y, Loizidou M, Seifalian AM (2009) Liposomes and nanoparticles: nanosized vehicles for drug delivery in cancer. Trends Pharmacol Sci 30:592–599
8. Carter JD, Cheng NN, Qu Y, Suarez GD, Guo T (2007) Nanoscale energy deposition by X-ray absorbing nanostructures. J Phys Chem B 111:11622–11625
9. Liu C-J et al (2010) Enhancement of cell radiation sensitivity by pegylated gold nanoparticles. Phys Med Biol 55:931–945
10. Hainfeld JF, Slatkin DN, Smilowitz HM (2004) The use of gold nanoparticles to enhance radiotherapy in mice. Phys Med Biol 49:N309–N315
11. Kobayashi K, Usami N, Porcel E, Lacombe S, Le Sech C (2010) Enhancement of radiation effect by heavy elements. Mutat Res 704:123–131
12. Usami N et al (2008) Mammalian cells loaded with platinum-containing molecules are sensitized to fast atomic ions. Int J Radiat Biol 84:603–611
13. Porcel E, Kobayashi K, Usami N, Remita H, Le Sech C, Lacombe S (2011) Photosensitization of plasmid-DNA loaded with platinum nano-particles and irradiated by low energy X-rays. J Phys Conf Ser 261:012004
14. Asharani PV, Wu, YL, Gong Z, Valiyaveettil S (2008) Toxicity of silver nanoparticles in zebrafish models. Nanotechnology 19:255102
15. Porcel E et al (2014) Gadolinium-based nanoparticles to improve the hadrontherapy performances. Nanomed Nanotechnol 10:1601–1608
16. Alric C et al (2008) Gadolinium chelate coated gold nanoparticles as contrast agents for both X-ray computed tomography and magnetic resonance imaging. J Am Chem Soc 130:5908–5915
17. Barreto JA, O'Malley W, Kubeil M, Graham B, Stephan H, Spiccia L (2011) Nanomaterials: applications in cancer imaging and therapy. Adv Mater 23:H18–H40
18. Alric C et al (2013) The biodistribution of gold nanoparticles designed for renal clearance. Nanoscale 5:5930–5939
19. Sancey L et al (2014) The use of theranostic gadolinium-based nanoprobes to improve radiotherapy efficacy. Br J Radiol 87:20140134
20. Albanese A, Tang PS, Chan WCW (2012) The effect of nanoparticle size, shape, and surface chemistry on biological systems. Annu Rev Biomed Eng 14:1–16
21. Chithrani BD, Ghazani AA, Chan WCW (2006) Determining the size and shape dependence of gold nanoparticle uptake into mammalian cells. Nano Lett 6:662–668
22. Zhang S, Li J, Lykotrafitis G, Bao G, Suresh S (2009) Size-dependent endocytosis of nanoparticles. Adv Mater 21:419–424

23. Perrault SD, Walkey C, Jennings T, Fischer HC, Chan WCW (2009) Mediating tumor targeting efficiency of nanoparticles through design. Nano Lett 9:1909–1915
24. Zhu M, Nie G, Meng H, Xia T (2012) Physicochemical properties determine nanomaterial cellular uptake, transport, and fate. Acc Chem Res 46:622–631
25. Lin Y, McMahon SJ, Paganetti H, Schuemann J (2015) Biological modeling of gold nanoparticle enhanced radiotherapy for proton therapy. Phys Med Biol 60:4149–4168
26. Beddoes CM, Case CP, Briscoe WH (2015) Understanding nanoparticle cellular entry: a physicochemical perspective. Adv Col Interface Sci 218:48–68
27. Hirsch V, Salaklang J, Rothen-Rutishauser B, Petri-Fink A (2013) Influence of serum supplemented cell culture medium on colloidal stability of polymer coated iron oxide and polystyrene nanoparticles with impact on cell interactions in vitro. IEEE Trans Magn 49:402–407
28. Yah CS (2013) The toxicity of gold nanoparticles in relation to their physiochemical properties. Biomed Res 24:400–413
29. Kalay S, Blanchet C, Culha M (2014) Linear assembly and 3D networks of peptide modified gold nanoparticles. Turk J Chem 38:686–700
30. da Rocha EL, Caramori GF, Rambo CR (2013) Nanoparticle translocation through a lipid bilayer tuned by surface chemistry. Phys Chem Chem Phys 15:2282–2290
31. Akhter S, Ahmad MZ, Ahmad FJ, Storm G, Kok RJ (2012) Gold nanoparticles in theranostic oncology: current state-of-the-art. Expert Opin Drug Deliv 9:1225–1243
32. Ranganathan R et al (2012) Nanomedicine: towards development of patient-friendly drug-delivery systems for oncological applications. Int J Nanomed 7:1043–1060
33. Illes E et al (2014) PEGylation of surfacted magnetite core-shell nanoparticles for biomedical application. Colloid Surf A 460:429–440
34. Thierry B, Griesser HJ (2012) Dense PEG layers for efficient immunotargeting of nanoparticles to cancer cells. J Mater Chem 22:8810–8819
35. Otsuka H, Nagasaki Y, Kataoka K (2003) PEGylated nanoparticles for biological and pharmaceutical applications. Adv Drug Deliv Rev 55:403–419
36. Chithrani BD, Stewart J, Allen C, Jaffray DA (2009) Intracellular uptake, transport, and processing of nanostructures in cancer cells. Nanomed Nanotechnol 5:118–127
37. Saptarshi SR, Duschl A, Lopata AL (2013) Interaction of nanoparticles with proteins: relation to bio-reactivity of the nanoparticle. J Nanobiotechnol 11:26
38. Shmeeda H, Tzemach D, Mak L, Gabizon A (2009) Her2-targeted pegylated liposomal doxorubicin: retention of target-specific binding and cytotoxicity after in vivo passage. J Controlled Release 136:155–160
39. Calvaresi EC, Hergenrother PJ (2013) Glucose conjugation for the specific targeting and treatment of cancer. Chem Sci 4:2319–2333
40. Gromnicova R et al (2013) Glucose-coated gold nanoparticles transfer across human brain endothelium and enter astrocytes in vitro. PLoS ONE 8:e81043
41. Hu C, Niestroj M, Yuan D, Chang S, Chen J (2015) Treating cancer stem cells and cancer metastasis using glucose-coated gold nanoparticles. Int J Nanomed 10:2065–2077
42. Dai Q, Walkey C, Chan WC (2014) Polyethylene glycol backfilling mitigates the negative impact of the protein corona on nanoparticle cell targeting. Angew Chem Int Ed 53:5093–5096
43. Miladi I et al (2014) The in vivo radiosensitizing effect of gold nanoparticles based MRI contrast agents. Small 10:1116–1124
44. Zhao P, Li N, Astruc D (2013) State of the art in gold nanoparticle synthesis. Coord Chem Rev 257:638–665
45. Turkevich J, Stevenson PC, Hillier J (1951) A study of the nucleation and growth processes in the synthesis of colloidal gold. Discuss Faraday Soc 11:55–75
46. Frens G (1973) Controlled nucleation for the regulation of the particle size in monodisperse gold suspensions. Nature 241:20–22
47. Brust M, Walker M, Bethell D, Schiffrin DJ, Whyman R (1994) Synthesis of thiol-derivatised gold nanoparticles in a two-phase liquid-liquid system. J Chem Soc Chem Commun 1994:801–802

48. Debouttiere P-J et al (2006) Design of gold nanoparticles for magnetic resonance imaging. Adv Funct Mater 16:2330–2339
49. Perrault SD, Chan WCW (2009) Synthesis and surface modification of highly monodispersed, spherical gold nanoparticles of 50–200 nm. J Am Chem Soc 131:17042–17043
50. Ahmadi T, Wang Z, Green T, Henglein A, El-Sayed M (1996) Shape-controlled synthesis of colloidal platinum nanoparticles. Science 272:1924–1926
51. Stepanov AL, Golubev AN, Nikitin SI, Osin YN (2014) A review on the fabrication and properties of platinum nanoparticles. Rev Adv Mater Sci 38:160–175
52. Miladi I et al (2013) Biodistribution of ultra small gadolinium-based nanoparticles as theranostic agent: application to brain tumors. J Biomater Appl 28:385–394
53. Faucher L, Tremblay M, Lagueux J, Gossuin Y, Fortin M-A (2012) Rapid synthesis of PEGylated ultrasmall gadolinium oxide nanoparticles for cell labeling and tracking with MRI. ACS Appl Mater Interfaces 4:4506–4515
54. Louis C et al (2005) Nanosized hybrid particles with double luminescence for biological labeling. Chem Mater 17:1673–1682
55. Torchilin VP, Papisov MI (1994) Why do polyethylene glycol-coated liposomes circulate so long? J Liposome Res 4:725–739
56. Nicol JR, Dixon D, Coulter JA (2015) Gold nanoparticle surface functionalization: a necessary requirement in the development of novel nanotherapeutics. Nanomedicine 10:1315–1326
57. Chattopadhyay N, Cai Z, Kwon YL, Lechtman E, Pignol J-P, Reilly RM (2013) Molecularly targeted gold nanoparticles enhance the radiation response of breast cancer cells and tumor xenografts to X-radiation. Breast Cancer Res Treat 137:81–91
58. Le Duc G et al (2011) Toward an image-guided microbeam radiation therapy using gadolinium-based nanoparticles. ACS Nano 5:9566–9574
59. Fang J et al (2014) Manipulating the surface coating of ultra-small Gd_2O_3 nanoparticles for improved T1-weighted MR imaging. Biomaterials 35:1636–1642
60. Bregoli L, Movia D, Gavigan-Imedio JD, Lysaght J, Reynolds J, Prina-Mello A (2016) Nanomedicine applied to translational oncology: a future perspective on cancer treatment. Nanomed Nanotechnol 12:81–103
61. Mignot A et al (2013) A top-down synthesis route to ultrasmall multifunctional Gd-based silica nanoparticles for theranostic applications. Chem Eur J 19:6122–6136
62. Tallury P, Payton K, Santra S (2008) Silica-based multimodal/multifunctional nanoparticles for bioimaging and biosensing applications. Nanomedicine 3:579–592
63. Stöber W, Fink A, Bohn E (1968) Controlled growth of monodisperse silica spheres in the micron size range. J Colloid Interface Sci 26:62–69
64. Ma K, Mendoza C, Hanson M, Werner-Zwanziger U, Zwanziger J, Wiesner U (2015) Control of ultrasmall sub-10 nm ligand-functionalized fluorescent core-shell silica nanoparticle growth in water. Chem Mater 27:4119–4133
65. Chi F, Guan B, Yang B, Liu Y, Huo Q (2010) Terminating effects of organosilane in the formation of silica cross-linked micellar core-shell nanoparticles. Langmuir 26:11421–11426
66. Arriagada FJ, Osseo-Asare K (1999) Synthesis of nanosize silica in a nonionic water-in-oil microemulsion: effects of the water/surfactant molar ratio and ammonia concentration. J Colloid Interface Sci 211:210–220
67. Patterson JP, Robin MP, Chassenieux C, Colombani O, O'Reilly RK (2014) The analysis of solution self-assembled polymeric nanomaterials. Chem Soc Rev 43:2412–2425
68. Zetasizer nano series user manual (2004)
69. Lehman SE, Tataurova Y, Mueller PS, Mariappan SVS, Larsen SC (2014) Ligand characterization of covalently functionalized mesoporous silica nanoparticles: an NMR toolbox approach. J Phys Chem C 118:29943–29951
70. Price WS (2005) Applications of pulsed gradient spin-echo NMR diffusion measurements to solution dynamics and organization. Diffus Fundam 2:112
71. Tomaszewska E et al (2013) Detection limits of DLS and UV-Vis spectroscopy in characterization of polydisperse nanoparticles colloids. J Nanomater 2013:313081

72. Pettitt ME, Lead JR (2013) Minimum physicochemical characterisation requirements for nanomaterial regulation. Environ Int 52:41–50
73. Morlieras J et al (2013) Development of gadolinium based nanoparticles having an affinity towards melanin. Nanoscale 5:1603–1615
74. Morlieras J et al (2013) Functionalization of small rigid platforms with cyclic RGD peptides for targeting tumors overexpressing $\alpha_v\beta_3$-integrins. Bioconjug Chem 24:1584–1597
75. Truillet C, Lux F, Tillement O, Dugourd P, Antoine R (2013) Coupling of HPLC with electrospray ionization mass spectrometry for studying the aging of ultrasmall multifunctional gadolinium-based silica nanoparticles. Anal Chem 85:10440–10447
76. Kotb S et al (2016) Gadolinium-based nanoparticles and radiation therapy for multiple brain melanoma metastases: proof of concept before phase I trial. Theranostics 6:418–427
77. Merbach A, Helm L, Toth E (2013) The chemistry of contrast agents in medical magnetic resonance imaging. Wiley
78. Davis ME, Shin DM (2008) Nanoparticle therapeutics: an emerging treatment modality for cancer. Nat Rev Drug Discov 7:771–782
79. Brigger I et al (2012) Nanoparticles in cancer therapy and diagnosis. Adv Drug Deliv Rev 64:24–36
80. Toulany M et al (2014) Cisplatin-mediated radiosensitization of non-small cell lung cancer cells is stimulated by ATM inhibition. Radiother Oncol 111:228–236
81. Liang K et al (2003) Sensitization of breast cancer cells to radiation by trastuzumab. Mol Cancer Ther 2:1113–1120
82. Hermanson GT (2013) Bioconjugate techniques. Academic Press
83. Conde J et al (2014) Revisiting 30 years of biofunctionalization and surface chemistry of inorganic nanoparticles for nanomedicine. Front Chem 2:48
84. Ghosh SS et al (1990) Use of maleimide-thiol coupling chemistry for efficient syntheses of oligonucleotide-enzyme conjugate hybridization probes. Bioconjug Chem 1:71–76
85. Lutz J-F, Zarafshani Z (2008) Efficient construction of therapeutics, bioconjugates, biomaterials and bioactive surfaces using azidealkyne "click" chemistry. Adv Drug Deliv Rev 60:958–970
86. Allen MP, Tildesley DJ (1989) Computer simulation of liquids. Oxford University Press
87. Frenkel D, Smit B (2001) Understanding molecular simulation: from algorithms to applications. Academic Press, San Diego
88. MacKerell AD Jr et al (1998) All-atom empirical potential for molecular modeling and dynamics studies of proteins. J Phys Chem B 102:3586–3616
89. Xiao F et al (2011) On the role of low-energy electrons in the radiosensitization of DNA by gold nanoparticles. Nanotechnology 22:465101
90. Verkhovtsev AV, Korol AV, Solov'yov AV (2015) Revealing the mechanism of the low-energy electron yield enhancement from sensitizing nanoparticles. Phys Rev Lett 114:063401
91. Hohenester U, Trügler A (2012) MNPBEM—A Matlab toolbox for the simulation of plasmonic nanoparticles. Comput Phys Commun 183:370–381
92. Palik ED (1998) Handbook of optical constants of solids. Academic Press
93. Alkilany AM, Murphy CJ (2010) Toxicity and cellular uptake of gold nanoparticles: what we have learned so far? J Nanopart Res 12:2313–2333
94. Boisselier E, Astruc D (2009) Gold nanoparticles in nanomedicine: preparations, imaging, diagnostics, therapies and toxicity. R Soc Chem 38:1759–1782
95. Bianchi A et al (2014) Quantitative biodistribution and pharmacokinetics of multimodal gadolinium-based nanoparticles for lungs using ultrashort TE MRI. Magn Reson Mater Phys Biol Med 27:303–316
96. Pan Y et al (2009) Gold nanoparticles of diameter 1.4 nm trigger necrosis by oxidative stress and mitochondrial damage. Small 5:2067–2076
97. Pan Y et al (2007) Size-dependent cytotoxicity of gold nanoparticles. Small 3:1941–1949
98. Nidome T et al (2006) PEG-modified gold nanorods with a stealth character for in vivo applications. J Control Release 114:343–347

99. Patra HK, Banerjee S, Chaudhuri U, Lahiri P, Dasgupta AK (2007) Cell selective response to gold nanoparticles. Nanomed Nanotechnol 3:111–119
100. Holmes P, Tuckett C (2000) Airborne particles: exposure in the home and health effects. MRC Institute for Environment and Health, Leicester
101. Wallace BA, Janes RW (2001) Synchrotron radiation circular dichroism spectroscopy of proteins: secondary structure, fold recognition and structural genomics. Curr Opin Chem Biol 5:567–571
102. Wallace BA (2000) Synchrotron radiation circular-dichroism spectroscopy as a tool for investigating protein structures. J Synchrotron Radiat 7:289–295
103. World Health Organization. http://www.who.int/mediacentre/factsheets/fs297/en/, http://www.who.int/mediacentre/factsheets/fs334/en/
104. Cancer Research UK. http://www.cancerresearchuk.org/about-cancer/type/
105. American Cancer Society. http://www.cancer.org/cancer/index
106. Wingfield C (2002) Skin cancer: an overview of assessment and management. Primary Health Care 22:28–37
107. Coulter JA et al (2012) Cell type-dependent uptake, localization, and cytotoxicity of 1.9 nm gold nanoparticles. Int J Nanomed 7:2673–2685
108. Lodish H, Berk A, Zipursky SL, Matsudaira P, Baltimore D, Darnell JE (2000) Molecular cell biology. W.H. Freeman, New York
109. Shukla R et al (2005) Biocompatibility of gold nanoparticles and their endocytotic fate inside the cellular compartment: a microscopic overview. Langmuir 21:10644–10654
110. Brust M et al (1995) Synthesis and reactions of functionalized gold nanoparticles. J Chem Soc Chem Commun 1995:1655–1656
111. Chithrani BD et al (2007) Elucidating the mechanism of cellular uptake and removal of protein-coated gold nanoparticles of different sizes and shapes. Nano Lett 7:1542–1550
112. Ivanov AI (2014) Pharmacological inhibitors of exocytosis and endocytosis: novel bullets for old targets. Methods Mol Biol 1174:3–18
113. Gao H et al (2013) Ligand modified nanoparticles increases cell uptake, alters endocytosis and elevates glioma distribution and internalization. Sci Rep 3:2534
114. Rogers DWO (1991) The role of Monte Carlo simulation of electron transport in radiation dosimetry. Appl Radiat Isot 42:965–974
115. Paganetti H et al (2004) Accurate Monte Carlo simulations for nozzle design, commissioning and quality assurance for a proton radiation therapy facility. Med Phys 31:2107–2118
116. Friedland W et al (1998) Monte Carlo simulation of the production of short DNA fragments by low-linear energy transfer radiation using higher-order DNA models. Radiat Res 150:170–182
117. Nikjoo H et al (2002) Modelling of DNA damage induced by energetic electrons (100 eV to 100 keV). Radiat Prot Dosim 99:77–80
118. Pimblott SM, Mozumder A (1991) Structure of electron tracks in water. 2. Distribution of primary ionizations and excitations in water radiolysis. J Phys Chem 95:7291–7300
119. Champion C et al (2012) EPOTRAN: a full-differential Monte Carlo code for electron and positron transport in liquid and gaseous water. Int J Radiat Biol 88:54–61
120. Incerti S et al (2010) Comparison of GEANT4 very low energy cross section models with experimental data in water. Med Phys 37:4692–4708
121. Muñoz A, Pérez JM, García G, Blanco F (2005) An approach to Monte Carlo simulation of low-energy electron and photon interactions in air. Nucl Instr Meth A 536:176–188
122. Krämer M, Durante M (2010) Ion beam transport calculations and treatment plans in particle therapy. Eur Phys J D 60:195–202
123. García Gomez-Tejedor G, Fuss MC (eds) (2012) Radiation damage in biomolecular systems. Springer
124. Nikjoo H et al (2012) Interaction of radiation with matter, CRC Press
125. Muñoz A et al (2008) Single electron tracks in water vapour for energies below 100 eV. Int J Mass Spectrom 277:175–179
126. Wälzlein C et al (2014) Low energy electron transport in non-uniform media. Nucl Instr Meth B 320:75–82

127. Waelzlein C et al (2014) Simulation of dose enhancement for heavy atom nanoparticles irradiated by protons. Phys Med Biol 59:1441–1458
128. Surdutovich E, Solov'yov AV (2014) Multiscale approach to the physics of radiation damage with ions. Eur Phys J D 68:353
129. de Vera P, Garcia-Molina R, Abril I, Solov'yov AV (2013) Semiempirical model for the ion impact ionization of complex biological media. Phys Rev Lett 110:148104
130. de Vera P, Abril I, Garcia-Molina R, Solov'yov AV (2013) Ionization of biomolecular targets by ion impact: input data for radiobiological applications. J Phys Conf Ser 438:012015
131. Surdutovich E, Solov'yov AV (2015) Transport of secondary electrons and reactive species in ion tracks. Eur Phys J D 69:193
132. Toulemonde M, Surdutovich E, Solov'yov AV (2009) Temperature and pressure spikes in ion-beam cancer therapy. Phys Rev E 80:031913
133. Surdutovich E, Solov'yov AV (2010) Shock wave initiated by an ion passing through liquid water. Phys Rev E 82:051915
134. Surdutovich E, Yakubovich AV, Solov'yov AV (2013) DNA damage due to thermomechanical effects caused by heavy ions propagating in tissue. Nucl Instr Meth B 314:63–65
135. de Vera P, Currell FJ, Mason NJ, Solov'yov AV (2016) Molecular dynamics study of accelerated ion-induced shock waves in biological media. Eur Phys J D 70:183
136. Surdutovich E, Yakubovich AV, Solov'yov AV (2013) Biodamage via shock waves initiated by irradiation with ions. Sci Rep 3:1289
137. Yakubovich AV, Surdutovich E, Solov'yov AV (2012) Thermomechanical damage of nucleosome by the shock wave initiated by ion passing through liquid water. Nucl Instr Meth B 279:135–139
138. Yakubovich AV, Surdutovich E, Solov'yov AV (2012) Damage of DNA backbone by nanoscale shock waves. J Phys Conf Ser 373:012014
139. Roots R, Okada S (1972) Protection of DNA molecules of cultured mammalian cells from radiation-induced single-strand scissions by various alcohols and SH compounds. Int J Radiat Biol Relat Stud Phys Chem Med 21:329–342
140. Hirayama R et al (2009) Contributions of direct and indirect actions in cell killing by high-LET radiations. Radiat Res 171:212–218
141. LaVerne JA (2000) Track effects of heavy ions in liquid water. Radiat Res 153:487–496
142. Plante I, Cucinotta F (2008) Ionization and excitation cross sections for the interaction of HZE particles in liquid water and application to Monte Carlo simulation of radiation tracks. New J Phys 10:125020
143. Friedland W, Jacob P, Bernhardt P, Paretzke HG, Dingfelder M (2003) Simulation of DNA damage after proton irradiation. Radiat Res 159:401–410
144. Karamitros M et al (2014) Diffusion-controlled reactions modeling in Geant4-DNA. J Comput Phys 274:841–882
145. Gervais B, Beuve M, Olivera GH, Galassi ME (2006) Numerical simulation of multiple ionization and high LET effects in liquid water radiolysis. Radiat Phys Chem 75:493–513
146. Von Sonntag C (2007) Free-radical-induced DNA damage as approached by quantum-mechanical and Monte Carlo calculations: an overview from the standpoint of an experimentalist. In: Sabin JR, Brändas E (eds) Advances in quantum chemistry, vol 52. Academic Press, pp. 5–20
147. Hirayama R et al (2013) OH radicals from the indirect actions of X-rays induce cell lethality and mediate the majority of the oxygen enhancement effect. Radiat Res 180:514–523
148. Sicard-Roselli C et al (2014) A new mechanism for hydroxyl radical production in irradiated nanoparticle solutions. Small 10:3338–3346
149. Paudel N, Shvydka D, Parsai EI (2015) Comparative study of experimental enhancement in free radical generation against Monte Carlo modeled enhancement in radiation dose deposition due to the presence of high Z materials during irradiation of aqueous media. Int J Med Phys Clin Eng Radiat Oncol 4:300–307
150. Zhang X-D et al (2009) Irradiation stability and cytotoxicity of gold nanoparticles for radiotherapy. Int J Nanomed 4:165–173

151. Sanche L (2008) Low energy electron damage to DNA. In: Shukla M, Leszczynski J (eds) Radiation induced molecular phenomena in nucleic acids, vol 5. Springer, Netherlands, pp 531–575
152. Sanche L (2005) Low energy electron-driven damage in biomolecules. Eur Phys J D 35:367–390
153. Sanche L (2009) Biological chemistry: beyond radical thinking. Nature 461:358–359
154. Lu Q-B (2010) Effects and applications of ultrashort-lived prehydrated electrons in radiation biology and radiotherapy of cancer. Mutat Res 704:190–1999
155. Fuss MC et al (2014) Current prospects on low energy particle track simulation for biomedical applications. Appl Radiat Isot 83B:159–164
156. Elsässer T, Cunrath R, Krämer M, Scholz M (2008) Impact of track structure calculations on biological treatment planning in ion radiotherapy. New J Phys 10:075005
157. Cobut V et al (1998) Monte Carlo simulation of fast electron and proton tracks in liquid water—I. Physical and physicochemical aspects. Radiat Phys Chem 51:229–243
158. Tennyson J (2010) Electron-molecule collision calculations using the R-matrix method. Phys Rep 491:29–76
159. Blanco F, Garcia G (2015) Interference effects in the electron and positron scattering from molecules at intermediate and high energies. Chem Phys Lett 635:321–327
160. Pimblott SM, Laverne JA (2007) Production of low-energy electrons by ionizing radiation. Radiat Phys Chem 76:1244–1247
161. Garrett WR (1975) Molecular scattering: convergence of close-coupling expansions in the presence of many open channels. Phys Rev A 11:1297–1302
162. Blanco F, Ellis-Gibbings L, Garcia G (2016) Screening corrections for the interference contributions to the electron and positron scattering cross sections from polyatomic molecules. Chem Phys Lett 645:71–75
163. Massey HSW, Burhop EHS, Gilbody HB (1970) Electronic and ionic impact phenomena, 2nd edn. In: Electron collisions with molecules and photo-ionization, vol 2. American Association for the Advancement of Science
164. Blanco F, Garcia G (2003) Improvements on the quasifree absorption model for electron scattering. Phys Rev A 67:022701
165. Blanco F, Garcia G (2004) Screening corrections for calculation of electron scattering differential cross sections from polyatomic molecules. Phys Lett A 330:230–237
166. Colmenares R, Sanz AG, Fuss MC, Blanco F, Garcia G (2014) Stopping power for electrons in pyrimidine in the energy range 20–3000 eV. Appl Radiat Isot 83B:91–94
167. Oller JC, Ellis-Gibbings L, da Silva FF, Limao-Vieira P, Garcia G (2015) Novel experimental setup for time-of-flight mass spectrometry ion detection in collisions of anionic species with neutral gas-phase molecular targets. EPJ Tech Instr 2:13
168. Jaffke T, Meinke M, Hashemi R, Christophorou LG, Illenberger E (1992) Dissociative electron attachment to singlet oxygen. Chem Phys Lett 193:62–68
169. Belic DS, Hall RI (1981) Dissociative electron attachment to metastable oxygen ($a^1\Delta g$). J Phys B At Mol Phys 14:365–373
170. Hayashi S, Kuchitsu K (1976) Elastic scattering of electrons by molecules at intermediate energies. Calculation of double scattering effects in N_2 and P_4. Chem Phys Lett 41:575–579
171. Almeida D et al (2012) Mass spectrometry of anions and cations produced in $1-4$ keV H^-, O^-, and OH^- collisions with nitromethane, water, ethanol, and methanol. Int J Mass Spectrom 311:7–16
172. Štefančíková L et al (2014) Cell localisation of gadolinium-based nanoparticles and related radiosensitising efficacy in glioblastoma cells. Cancer Nanotechnol 5:6
173. Harrison KG, Lucas MW (1970) Secondary electron energy spectra from foils under light-ion bombardment. Phys Lett A 33:142
174. Casta R, Champeaux J-P, Sence M, Moretto-Capelle P, Cafarelli P (2015) Comparison between gold nanoparticle and gold plane electron emissions: a way to identify secondary electron emission. Phys Med Biol 60:9095–9106

175. Haberland H, Karrais M, Mall M, Thurner Y (1992) Thin films from energetic cluster impact: a feasibility study. J Vac Sci Technol A 10:3266–3271
176. Kamalou O (2008) PhD Thesis, University of Caen
177. Alpen EL (1998) Radiation biophysics. Academic Press
178. Schardt D, Elsässer T, Schulz-Ertner D (2010) Heavy-ion tumor therapy: physical and radiobiological benefits. Rev Mod Phys 82:383–425
179. Verkhovtsev AV, Korol AV, Solovyov AV (2015) Electron production by sensitizing gold nanoparticles irradiated by fast ions. J Phys Chem C 119:11000–11013
180. Usami N, Kobayashi K, Furusawa Y, Frohlich H, Lacombe S, Le Sech C (2007) Irradiation of DNA loaded with platinum containing molecules by fast atomic ions C^{6+} and Fe^{26+}. Int J Radiat Biol 83:569–576
181. Butterworth KT, McMahon SJ, Currell FJ, Prise KM (2012) Physical basis and biological mechanisms of gold nanoparticle radiosensitization. Nanoscale 4:4830–4838
182. Misawa M, Takahashi J (2011) Generation of reactive oxygen species induced by gold nanoparticles under x-ray and UV irradiations. Nanomed Nanotechnol 7:604–614
183. Jain S et al (2011) Cell-specific radiosensitization by gold nanoparticles at megavoltage radiation energies. Int J Radiat Oncol Biol Phys 79:531–539
184. Chithrani DB et al (2010) Gold nanoparticles as radiation sensitizers in cancer therapy. Radiat Res 173:719–728
185. McMahon SJ, Mendenhall M, Jain S, Currell F (2008) Radiotherapy in the presence of contrast agents: a general figure of merit and its application to gold nanoparticles. Phys Med Biol 53:5635–5651
186. Ando K, Kase Y (2009) Biological characteristics of carbon-ion therapy. Int J Radiat Biol 85:715–728
187. Furusawa Y et al (2000) Inactivation of aerobic and hypoxic cells from three different cell lines by accelerated (3)He-, (12)C- and (20)Ne-ion beams. Radiat Res 154:485–496
188. Hirayama R, Furusawa Y, Fukawa T, Ando K (2005) Repair kinetics of DNA-DSB induced by X-rays or carbon ions under oxic and hypoxic conditions. J Radiat Res 46:325–332
189. Nakano T et al (2006) Carbon beam therapy overcomes the radiation resistance of uterine cervical cancer originating from hypoxia. Clin Cancer Res 12:2185–2190
190. Combs SE et al (2012) PhaseI/II trial evaluating carbon ion radiotherapy for the treatment of recurrent rectal cancer: the PANDORA-01 trial. BMC Cancer 12:137
191. Hirayama R et al (2013) Evaluation of SCCVII tumor cell survival in clamped and non-clamped solidtumors exposed to carbon-ion beams in comparison to X-rays. Mutat Res 756:146–151
192. Rothkamm K, Barnard S, Moquet J, Ellender M, Rana Z, Burdak-Rothkamm S (2015) DNA damage foci: meaning and significance. Environ Mol Mutagen 56:491–504